The HSP90/R2TP quaternary chaperone scaffolds assembly of the TSC complex

Claire Abeza, Philipp Busse, Ana C.F. Paiva, Marie-Eve Chagot, Justine Schneider, Marie-Cécile Robert, Franck Vandermoere, Christine Schaeffer, Bruno Charpentier, Pedro M. F. Sousa, et al.

Journal Pre-proofs

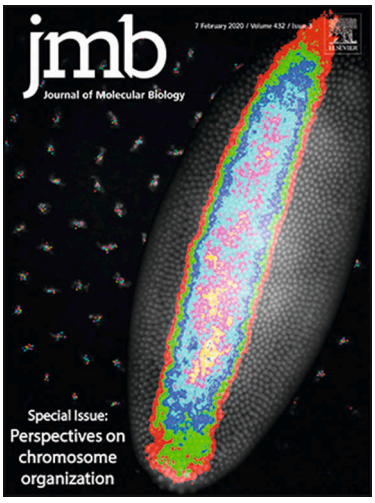

Research Article

The HSP90/R2TP quaternary chaperone scaffolds assembly of the TSC complex

Claire Abéza, Philipp Busse, Ana C.F. Paiva, Marie-Eve Chagot, Justine Schneider, Marie-Cécile Robert, Franck Vandermoere, Christine Schaeffer, Bruno Charpentier, Pedro M. F. Sousa, Tiago M. Bandeiras, Xavier Manival, Sarah Cianferani, Edouard Bertrand, Céline Verheggen

PII: S0022-2836(24)00469-8
DOI: https://doi.org/10.1016/j.jmb.2024.168840
Reference: YJMBI 168840

To appear in: *Journal of Molecular Biology*

Received Date: 17 September 2024
Revised Date: 22 October 2024
Accepted Date: 23 October 2024

Please cite this article as: C. Abéza, P. Busse, A.C.F. Paiva, M-E. Chagot, J. Schneider, M-C. Robert, F. Vandermoere, C. Schaeffer, B. Charpentier, P. M. F. Sousa, T.M. Bandeiras, X. Manival, S. Cianferani, E. Bertrand, C. Verheggen, The HSP90/R2TP quaternary chaperone scaffolds assembly of the TSC complex, *Journal of Molecular Biology* (2024), doi: https://doi.org/10.1016/j.jmb.2024.168840

The HSP90/R2TP quaternary chaperone scaffolds assembly of the TSC complex

Claire Abéza[1,2,3], Philipp Busse[4,5], Ana C.F. Paiva[4,5], Marie-Eve Chagot[6], Justine Schneider[7], Marie-Cécile Robert[1,2,3], Franck Vandermoere[8], Christine Schaeffer[7], Bruno Charpentier[6], Pedro M. F. Sousa[4], Tiago M. Bandeiras[4], Xavier Manival[6], Sarah Cianferani[7], Edouard Bertrand[1,2,3*] and Céline Verheggen[1,2,3*]

[1]IGMM, CNRS, Univ Montpellier, Montpellier, France.

[2] Equipe labellisée Ligue Nationale Contre le Cancer, Montpellier, France.

[3] IGH, CNRS, Univ Montpellier, Montpellier, France

[4] iBET, Instituto de Biologia Experimental e Tecnologica, Apartado 12, Oeiras, 2781-901, Portugal

[5] Instituto de Tecnologia Química e Biológica António Xavier, Universidade Nova de Lisboa, Av. da República, 2780-157 Oeiras, Portugal.

[6] Université de Lorraine, CNRS, IMoPA, F-54000 Nancy, France

[7] LSMBO, IPHC, Université de Strasbourg, CNRS UMR7178, Strasbourg, France

[8] IGF, CNRS, INSERM, Univ Montpellier, Montpellier, France

*: co-corresponding authors

Correspondence : edouard.bertrand@igh.cnrs.fr and celine.verheggen@igh.cnrs.fr

Running title: Assembly of TSC complex by HSP90/R2TP

Abstract

The R2TP chaperone is composed of the RUVBL1/RUVBL2 AAA+ ATPases and two adapter proteins, RPAP3 and PIH1D1. Together with HSP90, it functions in the assembly of macromolecular complexes that are often involved in cell proliferation. Here, proteomic

experiments using the isolated PIH domain reveals additional R2TP partners, including the Tuberous Sclerosis Complex (TSC) and many transcriptional complexes. The TSC is a key regulator of mTORC1 and is composed of TSC1, TSC2 and TBC1D7. We show a direct interaction of TSC1 with the PIH phospho-binding domain of PIH1D1, which is, surprisingly, phosphorylation independent. Via the use of mutants and KO cell lines, we observe that TSC2 makes independent interactions with HSP90 and the TPR domains of RPAP3. Moreover, inactivation of PIH1D1 or the RUVBL1/2 ATPase activity inhibits the association of TSC1 with TSC2. Taken together, these data suggest a model in which the R2TP recruits TSC1 via PIH1D1 and TSC2 via RPAP3 and HSP90, and use the chaperone-like activities of RUVBL1/2 to stimulate their assembly.

Keywords:

Tuberous sclerosis complex (TSC)/ heat shock protein 90 (HSP90)/ R2TP/ ATPases associated with diverse cellular activities (RUVBL1/2)/ protein-protein interaction

Introduction

Many cellular machineries are composed of multiple subunits. During their biogenesis, these subunits have to assemble with each other to become functional. However, unassembled subunits may be present in low amounts in the cell and pairwise interactions may also be too unstable to enable efficient formation of larger complexes. Chaperones and assembly factors are thus often needed to help the formation of complex cellular machines. HSP90 is a chaperone that works on a large spectrum of client proteins and often contributes to their folding at a late stage (1-3). It uses the energy generated by ATP hydrolysis to carry out its chaperoning functions, working as an ATP-dependent molecular pincer. In the apo form the pincer is open, however, when loaded with ATP, it adopts a closed conformation that traps its clients. ATP hydrolysis then drives client release (4). The ATPase cycle of HSP90 is regulated by numerous co-chaperones that help in the recruitment of specific clients (1,5). The R2TP complex is one of the most sophisticated HSP90 co-chaperone (6-8). It is composed of four subunits and it has some chaperone activity on its own (9, for a review). Most interestingly, the HSP90/R2TP chaperone system uniquely promotes the quaternary folding of multi-subunit cellular machineries (8,10). Indeed, it was shown to promote the assembly of the three nuclear RNA polymerases, the PIKK kinase complexes such as mTORCs, and many RNP complexes such as C/D and H/ACA snoRNPs, U4 and U5 snRNPs, and complexes involved in dsRNA metabolism (11-16). The R2TP is composed of RPAP3, PIH1D1, and the AAA+ ATPases RUVBL1/RUVBL2. In human, R2TP further associates with a set of prefoldins and prefoldin-like subunits to form the PAQosome (8,10). RUVBL1/2 form hetero-hexameric and dodecameric rings, and, compared to other AAA+ ATPases, have an additional domain called domain II (D_{II}). This domain locates on one side of the ring and its conformational change is believed to play key roles in the chaperone activity of R2TP (7, 17). Human RPAP3 possesses several distinct domains: an N-terminal domain that associates with the prefoldin-associated WDR92 protein (also known as Monad); two TPR domains binding HSP70 and HSP90; and a C-terminal domain that anchors it to the RUVBL1/2 ring, at the opposite side of their D_{II} domain (17-20). In addition, a short motif located downstream of TPR2 facilitates a stable interaction with PIH1D1 (6,20). RPAP3 is thus a central organizer of the R2TP complex (6,17,19). PIH1D1 can also interact with the D_{II} of the RUVBL1/2, but this interaction is labile and likely dynamic during the action of R2TP (7).

The R2TP is known to associate with co-factors that help in the recruitment of certain clients, such as TELO2 for PIKKs; NOPCHAP1, ZNHIT6 and the NUFIP1:ZNHIT3 heterodimer for C/D snoRNPs (11,12,21,22); ZNHIT2 and ECD for the U5 snRNP (13,15,23). Of note, RUVBL1/2 cofactors often belong to the Zf-HIT family (24). While some R2TP clients are recognized via co-factors, others make direct interactions with R2TP. In particular, the N-terminal domain of PIH1D1, called the PIH domain, contains a basic pocket that binds to phosphorylated acidic peptides of the DpSDDD/E consensus (21,25). In humans, a phosphorylated DSDED motif is found in EFTUD2, a U5 snRNP protein assembled by R2TP. This protein binds PIH1D1 but not a mutant of the PIH phospho-binding pocket (25), and the serine to alanine mutation in DSDED prevents the assembly of EFTUD2 in the U5 particles (15). A DSDDD/E motif is also found in ECD, a protein assisting U5 snRNP assembly (25); in TELO2, part of the TTT complex that chaperones PIKKs; and in MRE11, a protein of the MRN and MMAP complexes (26) and whose DSDDD/E motifs are required for stability and function (27). Other proteins such as RPB1 or UBR5 have also been reported to bind the PIH domain of PIH1D1 but whether they do so in a phospho-dependent manner is not clear (25,28). Interestingly, RPAP3 was recently shown to also directly recruit R2TP client proteins, as exemplified by the Dicer co-factor TRBP, an important actor of the miRNA biogenesis pathway

(29).

PIKKs are among the main R2TP clients (8). They form a family of six ubiquitous kinases/pseudo-kinases, ATM, ATR, DNAPK, mTOR, SMG1 and TRRAP, which play key roles in the cell. Interestingly, an interaction was recently described between R2TP and the Tuberous Sclerosis Complex (TSC; 13,15). The TSC is composed of TSC1 (Hamartin), TSC2 (Tuberin) and TBC1D7, and it is one of the main regulator of mTOR, the kinase that controls cell growth in response to resource availability. When nutrients are available, TSC is phosphorylated by the PI3K-AKT pathway (30). In this case, TSC is inactive and the small GTPase Rheb binds mTORC1 at the lysosomal membrane and activates it. In contrast, TSC becomes dephosphorylated when growth conditions are unfavorable. Dephosphorylated TSC then binds Rheb and inactivates it by stimulating its GTPase activity. Activation of the TSC thus leads to the formation of Rheb-GDP, mTORC1 inactivation and inhibition of cell growth (31). Importantly, genetic loss of TSC1 or TSC2 leads to a disease called Tuberous Sclerosis (32). In these patients, benign hamartomatous tumors form with a high frequency in the brain, skin, heart, kidneys and lungs. It however seems that the exorbitantly high mTORC1 activity observed in TSC deficient cells impedes the development of full blown tumors (33).

The cryo-EM structure of the human TSC was recently described and revealed an elongated, scorpion-like structure containing two copies of TSC1 and TSC2, and one of TBC1D7 (34,35). TSC2 has a GAP domain and TSC1 forms a long dimeric coiled-coil that scaffolds TSC2 and TBC1D7. A central helical domain in TSC1 can also mediate TSC1 oligomerization, which can then recruit six TSC2 molecules at the lysosomal membrane (36). This gives TSC1 a central role in TSC complex formation and function. In agreement, TSC1 was suggested to regulate the stability of TSC2 by facilitating its chaperone-dependent folding by HSP90 (37,38). Here, we identify a series of independent interactions between TSC subunits and the HSP90/R2TP chaperone, and we show that the R2TP stimulates the assembly of TSC2 with TSC1.

Results

The PIH domain of PIH1D1 associates with subunits of the TSC

The PIH1D1 N-terminal domain (PIH1D1_NTER, amino acids 1-180), also called the PIH domain, binds phosphorylated peptides with a DSDDD/E consensus (21,25; see Fig 1A). In order to more broadly identify the clients that bind this domain, we performed a quantitative, label-free proteomic study of GFP-PIH1D1 and GFP-PIH1D1_NTER that were expressed in Hela cells to a level close to endogenous one (Supp Fig1). To determine whether the phospho-binding pocket was involved in the interactions found, we also performed a pull-down using a mutant PIH domain that does not bind phospho-peptides (GFP-PIH1D1_NTER_K64A; 25). HeLa Flp-In cell lines were generated to stably express these GFP fusions and we performed anti-GFP immunoprecipitations (IPs) followed by mass-spectrometry (MS). RPAP3 and RUVBL1/2 were abundant in the PIH1D1 IP, as well as the prefoldin-like subunits present in the PAQosome (Fig 1B, Table S1). We also found many co-factors that directly bind RUVBL1/2, such as NOPCHAP1, DPCD and ZNHIT2. The TTT complex, another R2TP cofactor composed of TT1, TTI2 and TELO2 (which directly binds PIH1D1), was also enriched in the IP. Likewise, HSP90 and HSP70 and some of their cofactors were present, possibly via a direct binding to RPAP3 TPR domains (20). Numerous known and putative R2TP clients were also immunoprecipitated (Fig 1B), including subunits of the three nuclear RNA polymerases and other key transcriptional complexes (Mediator and Integrator), as well as proteins involved in membrane trafficking (TANGO6, SEC16A, EPS15L1). In the PIH1D1_NTER IP (Fig 1C), we did not detect RPAP3, RUVBL1/2, their co-factors and the prefoldin-like subunits. This was expected as the PIH domain does not bind other R2TP subunits (21). However, many R2TP clients were still immunoprecipitated. This was the case for RNA polymerase II subunits and the other Pol-II transcription complexes, and for the box C/D snoRNP core protein NOP56, NOP58 and FBL. Interestingly, direct comparison of the two IPs showed that a number of proteins bound the PIH1D1_NTER domain better than the full-length protein (Fig 1D). This was the case for the three subunits of the TSC complex (~4 times better), many factors involved in transcription (Mediator, Integrator, SUPT6H, RPRD1/2, with 4 to 100 fold better binding, see Table S1 for values). Moreover, some factors associated to the PIH1D1_NTER domain were not or very poorly associated to the full-length protein. Their association to the full length protein may be only very transient and the exogenous expression of PIH1D1_NTER, which is detached from the R2TP chaperone, may favor their detection in this IP. This was the case for the PAF and ELL complex involved in RNA polymerase II elongation, FIP1L1 and CDC73 that are involved in RNA 3'-end processing, and the RNA polymerase I initiation factors RRN3 and TCOF1. In contrast, some R2TP clients were bound solely or much more strongly than the fragment or mutant by the full-length PIH1D1 protein, like TANGO6, subunits of RNA polymerase III and proteins of the U5 snRNP.

Next, we wanted to determine the role of the phospho-peptide binding pocket of the PIH1D1_NTER domain. We compared wild-type and K64A mutant PIH domains, and observed that most R2TP clients were lost with the mutant (Fig 1E). This was the case for TELO2 as expected (39), for all the RNA polymerase subunits and the other transcription and RNA processing factors, as well as for the three TSC subunits. Only a small number of proteins remained associated with the mutant domain, SEC16A, ENGASE, EPS15L1 and few others (Fig 1E and Supp Fig 1C). These data indicate that the PIH1D1_NTER domain associates with many R2TP clients and partners, and that its phospho-binding pocket is important for most of these interactions. In particular, this is the case for the three subunits of the TSC complex, TSC1, TSC2 and TBC1D7.

TSC1 and TSC2 make independent interaction with PIH1D1 in an *in vivo* pair-wise assay

The PIKKs are key R2TP clients and since the TSC is a key regulator of mTOR, it was of high interest that it associated with PIH1D1. The TSC could regulate R2TP or, alternatively, could be assembled by it. We first set out to characterize in detail the interactions between TSC and R2TP. In order to define which TSC subunits bound PIH1D1, we used the LUMIER assay, which is a quantitative immunoprecipitation using pairs of over-expressed proteins (40). PIH1D1, PIH1D1_NTER and PIH1D1_NTER_K64A were fused to FLAG-tagged Firefly luciferase (3xFLAG-FL), while the three subunits of the TSC complex were fused to Renilla luciferase (RL). Plasmids were then transiently transfected in pair-wise combinations in HEK293 cells, and FL and RL activities were measured in the input and pellet after IP with anti-FLAG antibodies or without antibody as control. Co-IP efficiency was then defined as the IP/input ratio of RL relative to that of FL. RPAP3 and TELO2 were used as positive controls and ALIX as a negative one.

As expected, RL-RPAP3 was pulled-down by 3xFLAG-FL-PIH1D1 full-length but not the isolated 3xFLAG-FL-PIH domains (Fig 2A; 44% versus 0.2%). In contrast, RL-TELO2 was interacting with both 3xFLAG-FL-PIH1D1 and 3xFLAG-FL-PIHD1_NTER, but not with 3xFLAG-FL-PIH1D1_NTER_K64A (Fig 2A; 9.9% of efficiency for PIH1D1; 7.7% for PIH1D1_NTER and 0.5% for PIH1D1_NTER_K64A). This was consistent with the known ability of TELO2 to bind the PIH domain via its phosphorylated DpSDDE motif (25). A strong interaction was observed for TSC1 with PIH1D1 and PIH1D1_NTER, which was largely reduced by the K64A mutation of the PIH domain (Fig 2A; 8.7%, 12% and 2.9% of co-IP efficiency for PIH1D1, PIH1D1_NTER and the K64A mutant, respectively). TSC2 was only weakly pulled down with any of the PIH1D1 baits (Fig 2A; <2%). TBC1D7 did not show interaction for any of the three PIH1D1 baits (Fig 2A). Its presence in our proteomic analysis thus suggests an indirect association via the other TSC subunits.

In order to determine the regions of TSC1 responsible for PIH1D1 binding, we prepared TSC1 truncated mutants, taking into account its known interaction domains with TSC2, TBC1D7 and HSP90 (Fig 2B, 37, 41-45). We defined four TSC1 truncation mutants (TSC1_D1 to D4, Fig 2B), and fused them to RL to test their interactions with the PIH1D1 baits in LUMIER IPs (Fig 2C). We found that TSC1_D3, which contains a coil-coiled domain (CCD) involved in its dimerization, was efficiently pulled-down by PIH1D1 and PIH1D1_NTER, while this interaction was reduced with the K64A mutant (Fig 2C; 10% of efficiency for PIH1D1; 22.7% for PIH1D1_NTER and 2.7% for PIH1D1_NTER_K64A). Interestingly, PIH1D1_NTER also interacted with TSC1_D4, which share the coiled-coil domain with TSC1_D3. Binding was however reduced compared to D3, suggesting that the TSC1 coiled-coil domain is required for interaction with PIH1D1_NTER, but not sufficient as the interaction was strengthened by the 40 amino acids immediately upstream of it. Similarly, we tried to identify the regions of TSC2 interacting with PIH1D1. Four domains of TSC2 (TSC2_D1-D4) were generated and tested in LUMIER IPs, but none interacted with PIH1D1 or the PIH1D1_NTER domain (Supp Fig 2A and B). To confirm the data obtained by LUMIER IP assays, we tested the same interactions by two-hybrid assays (Supp Fig 2C). Again, the TSC1 domain 3 interacted strongly with PIH1D1_NTER and more weakly with PIH1D1_NTER K64A. Taken together, these data indicate that the TSC1 domain 3 binds PIH1D1 via the basic pocket of its PIH domain.

TSC1 domain 3 makes direct, phosphorylation independent interactions with the PIH1D1 N-terminal domain and RUVBL1/2

The PIH domain of PIH1D1 can bind phospho-peptides of the DpSDDD/E consensus. Therefore, we evaluated whether phosphorylation plays a role in the interaction of TSC1-D3 with the PIH domain. We first performed a phospho-proteomic analysis of the protein pelleted in the PIH1D1 and PIH1D1_NTER IPs. The mean number of phosphorylated peptides identified after a TiO2 purification column showed that much more phospho-peptides were present in the PIH1D1_NTER IP as compared to PIH1D1 and control IPs (813 vs. 119 and 0; Fig 3A and Table S2). However, these phospho-peptides did not show predominant DSDDD/E sequences (25). Moreover, although some TSC1 and TSC2 phospho-peptides were identified, none belonged to the TSC1_D3 that mediates strong binding to the PIH domain.

In order to directly test whether TSC1 phosphorylation was required for its interaction with PIH1D1-NTER, we performed LUMIER IP and subsequently treated the pellets with lambda phosphatase (Fig 3C). We used TELO2 as a control as it carries a phosphorylated DpSDDE sequence that mediates binding to the PIH domain (25). As expected, we found a 50% decrease in TELO2 binding to PIH1D1_NTER when lambda phosphatase was added. In contrast, this treatment has no effect on the binding of TSC1 to the PIH1D1_NTER, suggesting this interaction not to depend on TSC1 phosphorylation (Fig 3C). Similarly, the weak interaction of TSC2 with PIH1D1 was not affected. We also tested TSC1 domains D3 and D4. Although the interactions of these domains with PIH1D1_NTER were lower in these conditions that included a 30 min incubation at 30°C, the lambda phosphatase treatment had no effect (Fig 3C). Finally, we performed a co-expression assay in *E. coli* to determine whether TSC1 makes direct physical interactions with PIH1D1_NTER. We could not produce a soluble form of TSC1_D3 in *E. coli*, but a shorter form of TSC1_D4 expressed reasonably well (Fig 4A; TSC1_D4b, amino-acids 725-1047). Importantly, we observed that His-TSC1_D4b could pull down PIH1D1_NTER (Fig 4A; note that the identity of the bands was confirmed by mass spectrometry; Supp Fig 3). Taken together, these data demonstrate that TSC1 domains 3 and 4 interact directly with the PIH1D1 basic pocket in absence of phosphorylation, thereby revealing a new mode of interaction of PIH1D1 with client proteins.

It is also worth noting that TSC1 likely interacts with the remaining R2TP subunits, as we observed that TSC1 interacts with RUVBL1 by two-hybrid and with RUVBL1/2 and RPAP3 by LUMIER IP (Supp Fig 2C and D respectively). To demonstrate this mode directly, we co-expressed full length HIS-RUVBL1 and RUVBL2-FLAG-Fh8 together with His-Avi-TSC1(725-1047) and BirA. After induction of expression, biotin was added to the growth medium to ensure biotinylation of TSC1(725-1047). Proteins were then extracted and immobilized and HisTrap HP beads. Eluted proteins were analyzed by SDS PAGE for total protein detection as well as Western blotting against biotin to detect biotinylated TSC1(725-1047). Fractions showing co-elution of RUVBL1, RUVBL2 and TSC1(725-1047) were pooled and loaded onto a anti-Flag affinity gel, with the aim of capturing only the Flag-tagged RUVBL2. The affinity gel was extensively washed and the remaining proteins were then eluted from the Flag resin-bound proteins. This second step of complex purification ensured removal of all proteins that are not in a stable complex with RUVBL1/2. A negative control was done to show that TSC1 fragment and RUVBL1 can not bind non-specifically to anti-Flag beads (Supp Fig 3). Monitoring the input, wash, and eluted fractions was performed with anti-biotin, anti-His and anti-Flag Western blots to detect all the specific tags of RUVBL1, RUVBL2 and TSC1(725-1047) (Fig 4B). This demonstrated that TSC1(725-1047) and RUVBL1/2 co-eluted from the His-capture and Flag-capture purifications, which indicated the formation of a stable protein complex between all three proteins.

TSC2 interacts with PIH1D1 and other R2TP subunits in a TSC1 independent manner

The previous LUMIER IP experiments suggest a possible interaction of TSC2 with PIH1D1, but since this interaction is much weaker than the one of TSC1, it was not clear whether it was direct or mediated by TSC1. To clarify this, we knocked-out TSC1 in HEK 293T cells by CRISPR/Cas9. We verified the absence of TSC1 by genotyping and Western Blot in two clones (Fig 5A). No large change in cell cycle was observed in the KO cells (Supp Fig 4), and the levels of TSC2, PIH1D1 and RPAP3 were not affected (Fig 5A). Using LUMIER IPs, we measured the interactions of TSC2 with the different R2TP subunits, in wild-type and TSC1 KO cells. Interestingly, TSC2 showed an interaction with the all four subunits of R2TP, as well as with the isolated PIH1 domain of PIH1D1 (Fig 5C). In contrast to TSC1, this interaction was not affected by mutating the phospho-binding pocket.

To further characterize the interactions of TSC2 with R2TP, we knocked out PIH1D1 in HEK 293T cells by CRISPR/Cas9. Clones were genotyped and characterized by Western Blot and FACS analysis (Fig 5B and Supp Fig 4). Two clones showed absence of PIH1D1, and RPAP3 was equally expressed in these clones as compared to parental cells. We then used these KO clones to study the interactions of TSC2 by LUMIER IPs (Fig 5D). In parental cells, TSC2 was pulled down by RPAP3 and, to a lesser extent, by RUVBL1 and RUVBL2. Similar or slightly stronger interactions were observed in PIH1D1 KO cells. Thus, TSC2 interacted with RPAP3 and RUVBL1/2 proteins independently of PIH1D1.

To characterize in more details these interactions, we analyzed which domains of RPAP3 interacts with TSC2 and tested its C-terminal domain, which binds RUVBL1/2 (17,19), and its TPR domains (133-396), which binds HSP70/90 (20, and for a review, 8). We also prepared the RPAP3 TPR domains with a double mutation (N172A and N321A), which prevents binding to both HSP70/90 (20). Using LUMIER IPs, we found that the RPAP3 C-terminal domain immunoprecipitated TSC2 (Fig 6A). This could be indirect since TSC2 also interacts with RUVBL1/2 (Fig 5) and RPAP3 C-ter binds them strongly. Interestingly, TSC2 also interacted with the RPAP3 TRP domains, and binding was reduced by two fold when the TPRs were mutated (Fig 6A). Since the RPAP3 TPR domains do not associate with other R2TP proteins (20), this suggested that TSC2 could interact with the RPAP3 TPRs in two ways, either indirectly through HSP90 or HSP70, or directly through the TPRs themselves, as seen in the case of TRBP that associates with the RPAP3 TPRs at a site opposite to HSP90 (29). This possibility is attractive as it could explain how TSC2 could be channeled from HSP70 and HSP90 to RPAP3 and finally R2TP (see below).

TSC1 and TSC2 are clients of HSP90

TSC2 was recently shown to be stabilized by TSC1 with the help of HSP90 (37). R2TP binds HSP90 and the TSC/R2TP interaction data presented above prompted us to revisit the role of HSP90 on TSC1 and TSC2. To this end, we first performed a SILAC quantitative proteomic study of TSC2 partners (Fig 6B and Table S3). TSC2 was fused to GFP, stably expressed in HeLa cells and immunoprecipitated with anti-GFP antibodies. TSC1 was the main TSC2 partner as expected, but the HSP70 and HSP90 chaperones were also abundant in the IP, as well as some of their co-chaperones like BAG2 and STIP1. The R2TP subunits were not enriched above background, and this could be due to a transient association with R2TP during

the biogenesis of the TSC complex.

Next, we investigated the role of HSP90 in the biogenesis of TSC1 and TSC2. For this, we transfected TSC1 and TSC2 fused to RL in HEK 293T cells and measured their expression levels in cells treated or not with Geldanamycin, an inhibitor of HSP90 often leading to client degradation. We found that Geldanamycin did not alter expression of a series of control proteins (ALIX, CSRP2, MAP4, RTCB), but led to significantly decreased levels of RL-TSC1 and RL-TSC2 (40%, Fig 6C). This is similar to the effect observed to greater extent for NOP58, a protein already described to be destabilized by HSP90 inhibition (22). This shows that HSP90 is involved in stabilizing both TSC1 and TSC2, and that these proteins are probable clients of this chaperone.

R2TP via the RUVBL1/2 ATPase activity stimulates the assembly of the TSC complex

The complex and dense network of interactions between the TSC and R2TP complexes described above fits the hypothesis that the HSP90/R2TP chaperone could be involved in the assembly of the TSC, as it does for other macromolecular complexes (8). To directly test this possibility, we studied the association of TSC1 with TSC2 in conditions where R2TP is impaired. We first performed LUMIER IPs in PIH1D1 KO clones (Fig 7A). We found a 34% decrease in the interaction between 3XFLAG-FL-TSC1 and RL-TSC2 in PIH1D1 KO cells as compared to wild-type (Fig 7A, left). This effect in the absence of PIH1D1 was also observed when the interaction was tested in the other direction (e.g. 3XFLAG-FL-TSC2 with RL-TSC1; Fig 7A, right panel, 28% decrease), even though in these conditions the association of TSC1 with TSC2 is much more efficient (40% co-IP efficiency vs. 4%; compare left and right panels). Moreover, this effect was also visible when the TSC1_D3 and D4 were used as preys. Our data thus suggest that PIH1D1 favors association of TSC1 with TSC2.

Next, we tested the role of the RUVBL1/2 AAA+ ATPases, which are believed to have chaperone activity and to play a key role in promoting the assembly of macro-molecular complexes (8,9). We used the small compound CB-6644, which was recently developed and inhibits their ATPase activity (46). We performed TSC1/TSC2 LUMIER IPs and observed a 73% decrease of association of TSC2 with TSC1 in presence of CB-6644 (Fig 7B). Moreover, a cumulative effect of RUVBL1/2 inhibition with PIH1D1 KO was observed, leading up to a 90% reduction in the association of TSC1 with TSC2 in PIH1D1 KO cells treated with CB-6644 (Fig 7B). TBC1D7 did not significantly associated with TSC1 or TSC2 in this assay (Fig 7A and 7B), precluding the assessment of the effect of R2TP. Altogether, these data show that R2TP promotes the interaction between TSC1 and TSC2, and thus the assembly of the TSC complex. The stimulation of this interaction requires both PIH1D1 and the activity of the RUVBL1/2 ATPases, and at least in some instances, the effect of these factors is additive.

Discussion

The N-terminal domain of PIH1D1 plays a central role in TSC subunit recognition

The PIH domain of PIH1D1 possesses a basic pocket that binds phospho-peptides, and Lys57 and Lys64 are essential for these interactions (39). Previous proteomic analysis of full-length PIH1D1 and a K64A mutant showed that TELO2, EFTUD2, UBR5 and the RNA polymerase II subunit RPB1 were interacting with wild-type but not mutant PIH1D1 (25). In this study, we performed a proteomic analysis of the PIH domain of PIH1D1, wild-type or mutated on K64. We found that the wild-type PIH domain interacted with a large number of proteins including many not previously known to bind PIH1D1, such as the PAF, Mediator and Integrator transcriptional complex. Remarkably, almost all these partners were lost in the K64A mutant, except for a few factors like SEC16A, ENGASE and EPS15L1. Of special interest for this study, we observed a differential association of the TSC subunits (TSC1, TSC2 and TBC1D7), suggesting that the basic pocket of the PIH domain is involved in TSC binding.

The PIH domain binds phosphorylated peptide with a DpSDDD/E consensus motif (25). Nevertheless, this is probably not the unique feature recognized by this domain. Most PIH1D1 interactants do not have DSDDD/E or related motifs, such as RPB1 or UBR5, and this is also the case here for TSC subunits. Moreover, we showed that phosphorylation of TSC1 is not required for its interaction with PIH1D1 N-terminal domain, in cells and *in vitro* with recombinant proteins. Thus, while the interaction between TSC1 and PIH1D1 is direct and uses the PIH phospho-binding pocket, it is phosphorylation independent. The TSC1 domain that interacts with PIH1D1 contains the coiled-coil region and sequences immediately upstream of it (Fig 2 and 3, amino acids 725 to 1047 of TSC1). There is an acidic region at the C-terminal end of TSC1 that could insert in the basic pocket of the PIH domain. Unfortunately, deletion of this sequence only marginally affected its binding to PIH1D1 (Supp Fig 5). This suggests an entirely novel mode of interaction for the PIH domain.

The HSP90/R2TP chaperone acts as a platform to assemble the TSC complex

In this study, we used various assays in wild type, PIH1D1- and TSC1-KO cells to investigate in detail the interactions between R2TP and TSC. We discovered a complex and dense network of contacts linking these two complexes (see Fig 8A for a summary): (*i*) TSC1 domain 3 interacted with the phospho-binding pocket of the PIH domain of PIH1D1 (proteomics, LUMIER IPs, two-hybrid assays, *in vitro* assay); (*ii*) TSC2 associated with the same PIH1 domain but in a manner that was independent from the pocket or TSC1 (LUMIER IPs in TSC1 KO cells); (*iii*) TSC2 bound the RPAP3 TPR domains, both directly and via HSP90 (proteomics, LUMIER IPs); (*iv*) TSC1 interacted with RUVBL1/2 (LUMIER IPs, two-hybrid assay for RUVBL1 and *in vitro* assay).

Structural analysis of the TSC complex revealed an unexpected stoichiometry of 2:2:1 for TSC1, TSC2 and TBC1D7 (35). The TSC complex forms a scorpion-like structure, with the N-terminal and C-terminal domains of TSC1 being respectively the scorpion's pincer and tail. The tail binds TBC1D7, whose association stabilizes the entire TSC complex (34, 35,47). The scorpion central body is formed by a pseudo-symmetric TSC2 dimer, arranged in a tail-tail manner, and binding a dimer of the coiled-coil domains of TSC1. Importantly, the scorpion central body contains the key GAP (GTPase-Activating Protein) domain of TSC2, which is thus present in two copies and ideally placed to bind a pair of Rheb GTPase in mTORC1 (34,48). In

addition, an oligomeric structure of six molecules of TSC1 and TSC2 has also been described, in which TSC1 plays a central organizing role (36). These sophisticated super-structures, together with the numerous interactions described here, suggests that the R2TP could function as a platform to recruit and position the TSC subunits in order to facilitate their assembly. Indeed, we showed that the TSC1-TSC2 interaction, as measured by LUMIER IPs, were reduced in absence of PIH1D1. Moreover, the ATPase activity of RUVBL1/2 was also required, as the CB-6644 inhibitor also reduced association of TSC1 with TSC2. The effect of PIH1D1 removal and RUVBL1/2 inhibition were additive, leading up to 90% inhibition of TSC1/TSC2 interaction in some conditions (Fig 7). The ATPase cycle of RUVBL1/2 has been linked to large scale movements of their D_{II} domains (7,9). These movements could help moving TSC1 or TSC2, or domains of these proteins, and may favorize formation of the mature TSC complex.

HSP90 stabilizes TSC1 and TSC2, and helps TSC assembly

Many HSP90 inhibitors block its ATPase activity and freeze HSP90 on its client proteins, which are then degraded by the proteasome. Notably, it was demonstrated that inhibition of HSP90 leads to ubiquitination and degradation of TSC2, suggesting that it is a client of this chaperone (37). In agreement, a large amount of HSP90 and HSP70 bound GFP-TSC2 in our proteomic study. Moreover, TSC2 associated less efficiently to a RPAP3 TPR domains containing mutations that prevent HSP90 binding. All this provide strong evidence that TSC2 directly binds HSP90 and is a client of this chaperone.

It was previously described that TSC1 can act as a co-chaperone of HSP90, inhibiting its ATPase activity to facilitate client loading (37, 38). TSC1 directly binds the middle domain of HSP90, but binding also requires the MEEVD C-terminus of HSP90, although how this sequence stabilizes the interaction remains unclear (37). The direct binding of TSC1 to PIH1D1 could explain this additional requirement, as PIH1D1 is stably associated with RPAP3, which binds HSP90 MEEVD via its TPR domains (20). Because TSC1 inhibits HSP90 ATPase activity and helps client loading (37), TSC1 bound to the PIH1D1:RPAP3:HSP90 complex may maintain the chaperone open to help TCS2 loading (Fig 8B). The stoichiometry of the interactions also provides a model for how to assemble the TSC complex with the required 2:2 stoichiometry of TSC1 and TSC2. Indeed, HSP90 is a dimeric chaperone and each of its middle domain could bind a TSC1 monomer (37). Similarly, two TSC2 monomers could also be recruited by a dimeric HSP90, most likely with the help of RPAP3, and then be held together by the closure of HSP90 lid upon ATP binding (Fig 8C). This would facilitate assembly of the TSC1 and TSC2 dimers, most likely with the help of the ATPase activity of RUVBL1/2.

It is interesting to note that some signaling kinases such as Erk and IKKβ inactivate the TSC by inducing its dissociation (49,50). Likewise, the sub-cellular localization of TSC is tightly controlled (36). It localizes to lysosomes upon amino acid starvation and dissociates from this compartment upon nutrient abundance, enabling regulation of lysosomal mTORC1 (51). In the future, it will be interesting to investigate whether the HSP90/R2TP system promotes cycles of TSC dissociation/reassembly or contributes to its change in localization.

Coordinated biogenesis of PIKK and TSC by the HSP90/R2TP chaperone

HSP90 acts as a chaperone for a large number of clients involved in tumor initiation and

progression (1), and it is a suitable target for cancer therapy (52,53). It is thus interesting to note that the biogenesis of both TSC and mTORC1 depends on the HSP90/R2TP chaperone (39). By regulating the biogenesis of both complexes, the outcome of R2TP on the mTOR pathway includes positive and negative effects that could balance each other and limit HSP90/R2TP-dependent tumorigenesis (54). In this regards, it has been shown that some effects of mTORC1 hyperactivation caused by loss of TSC1/TSC2 can be reversed by HSP90 inhibition (54). It will be interesting in the future to determine if R2TP inhibition could also be used in the treatment of Tuberous Sclerosis, alone or in combination with HSP90 or mTOR inhibitor-based therapies.

Materials and methods

Cell culture and plasmid transfection

HeLa Flp-In cells were a gift of S. Emiliani (Institut Cochin, Paris and 55). HEK 293T cells were from the ATCC collection. All cells were grown at 37°C, 5% CO2 and plasmid transfections were done with JetPrime (Ozyme). HeLa Flp-In and HEK 293T cells were grown in Dulbecco's modified eagle medium (DMEM) containing 10% fetal bovine serum (FBS), glutamine (2.9 mg/mL), and penicillin/streptomycin (10 U/mL). Cells were regularly tested for mycoplasma contamination. For Label Free or SILAC experiments, HeLa Flp-In cells were co-transfected with Flippase O expression plasmid and pcDNA5-3×FLAG-GFP plasmid fused with protein of interest (PIH1D1 full-length protein, PIH1D1_NTER, PIH1D1_NTER_K64A, TSC2) with JetPrime reagent according to the manufacturer's protocol (Ozyme). Clones were selected in hygromycin B (150 µg/mL), picked individually and characterized by Western Blot and fluorescence microscopy. CRISPR/Cas9 knock-out cells were generated by transfection of HEK 293T cells expressing Flag-Cas9 with Sanger Lentiviral CRISPR vector plasmid U6-gRNA/PGK-puro-2A-BFP and guide RNA to the protein of interest (PIH1D1 and TSC1) or control locus according to the manufacturer's protocol (Sigma-Aldrich). Sequences of RNA guides are as following: TSC1-TGAAATAAGGGTGTCTGGTGTG and AGACGAAGTTGCAAGGGTACAT; PIH1D1-CACCGTTGACAGCTACGTCGTAGG and AAACCCTACGACGTAGCTGTCAACC. After selection with puromycin and blasticidin, one single-cell per well was sorted into 96-well plates by FACS for BFP expression, and clones KO for TSC1 were screened either by Western Blot or PCR and sequencing on genomic DNA.

Plasmids and cloning

DNA cloning was performed using standard techniques or with the Gateway™ system (InVitrogen). PIH1D1, RPAP3, TSC1 and TSC2 fragments were generated by PCR and cloned in pDon vector by BP reaction (Gateway). To generate GFP fusions for Label Free or SILAC-IPs, pcDNA5-FRT-GFP-3xFLAG-Rf was recombined with pDon vectors by LR reaction (Gateway). For the LUMIER-IP assays, recombination was done with pcDNA5-FRT-3xFLAG-FL-Rf for the bait, and L30-HA-RL-Rf for the prey. Most of cDNAs were from human origin except for RUVBL1 and RUVBL2 which were from mouse. For Yeast Double Hybrid experiments, baits and prey were transfected in pACTII and pAS2ΔΔ. TSC1 (725-1047) and PIH1D1 (1-180) fragments were cloned respectively into pnEA::3CH (ampicillin resistant) with a 6xHis N-terminal tag and pnCS (spectinomycin resistant) vectors (derived from the pET vector), using 5' *Nde*I and 3' *BamH*I restriction sites.

Antibodies

Primary antibodies and dilutions for Western Blots were the following: rabbit polyclonal anti-PIH1D1 (Proteintech 19427-1-AP) at 1:1000, rabbit polyclonal anti-RPAP3 (Sigma SAB1411438) at 1:1000, mouse monoclonal anti-GAPDH (Abcam ab8245) at 1:20000, rabbit monoclonal anti-TSC1 (CST #6935) at 1:1000, rabbit monoclonal anti-TSC2 (CST #4308) at 1:500, mouse anti-Tubulin, (I2G10) at 1:500. Secondary antibodies were goat anti-rabbit and goat anti-mouse coupled to HRP (Sigma).

Western Blot

Proteins were prepared by cell lysis in cold HNTG buffer (20 mM HEPES, pH 7.9, 150 mM NaCl, 1% Triton X-100, 10% Glycerol, 1 mM $MgCl_2$, 1 mM EGTA, and protease inhibitors (cOmplete, Roche)) and incubated for 20 min at 4°C. Protein concentration was determined by Bradford assay. Protein samples were mixed with Laemmli 2X buffer (4% SDS, 10% 2-mercaptoethanol, 20% glycerol, 0.004% bromophenol blue, 0.125 M Tris-HCl) and boiled for 5 min at 95°C. Protein lysates were separated by gradient 4%-15% SDS-PAGE (BioRad) and transferred to a PVDF membrane (Amersham Hybond, GE Healthcare). For Western Blot of KO cells, membranes were blocked with 2.5% fat milk (w/v) in Tris buffered Saline 1X with 0.05% Tween and incubated with the appropriate primary antibodies at the appropriate dilution and followed by incubation with secondary antibodies conjugated to HRP. Enzymatic activity was detected using the ECL kit (Roche).

LUMIER IPs

HEK 293T cells were seeded in 24-well plates at 150,000 cells per well and transfected with 450 ng of the RL fusion and 50 ng of the 3xFLAG-FFL fusion, with 1 µL of JetPrime (Ozyme), as recommended by the manufacturer and let for 48 h. When treated with CB-6644 (46) drug was added 4 h after transfection at 500 nM final. Cells were extracted in 500 µL of HNTG containing protease inhibitor cocktail (Roche) and centrifuge at 4°C and at 3,220 *x g* for 5 min. For IP, a high-binding 96-well plates (Lumitrac, High binding, Greiner 655074) was coated with 70 µL of M2 anti-FLAG antibody (10 µg/mL in 1× PBS; F1804 Sigma-Aldrich) and incubated overnight at room temperature (RT) in the dark. The next day, wells were blocked with 300 µl of blocking buffer (3% BSA, 5% sucrose, 0.5% Tween 20, 1× PBS), for 1 h at RT. 100 µL of each extract were dispatched in two wells, one for control without antibody and one with anti-FLAG antibody. Plates were incubated 3 h at 4°C and wells were washed 5 x 10 min with 300 µL of ice-cold HNTG. After the last wash, 10 µL of PLB lysis buffer (Promega) was added in each well. To measure the signal in the input, 2 µL of extract and 8 µL of PLB buffer was put in empty remaining wells. FL and RL luciferase activities were measured in IP and input wells, using the dual luciferase kit (Promega) to determine the % of IP efficiency (19). Each transfection and IP were done in duplicates within a 96-well plate. Experiments were additionally repeated multiple times as indicated in the Figure legends. In experiments done with HEK 293T KO clones, each transfection was done in parallel in KO cells and control HEK 293T cells. For lambda phosphatase assay, after IP and before wash steps, extracts were treated with 1,000 U of Lambda Protein Phosphatase (NEB P0753) or only its Buffer (10X NE Buffer Protein MetalloPhosphatases (PMP) and 10 mM $MnCl_2$) following manufactured protocol for 30 min at 30°C.

Luciferase assays

HEK 293T cells were grown on 24-well plates and co-transfected with 50 ng of plasmid expressing a 3XFLAG-tagged Firefly luciferase alone (3xFLAG-FL) and 450 ng of plasmid coding Renilla luciferase (RL) in fusion with the protein of interest with 1 µL of JetPrime (Ozyme). After 48 h, cells were extracted in 100 µL of PLB buffer (Promega) and incubated at

4°C for 15 min. RL and FL activities were measured on 96-well plates using 4 µL of cell extract and the dual-luciferase assay kit (Promega). Values obtained for RL were normalized to FL values. Each experiment was done in duplicate and repeated three times for statistics. When treated with Geldanamycin (GA, Sigma G3381), drug was added 16 h before extraction at 2 µM final.

SILAC labeling and proteomic analysis

HeLa Flp-In cells were grown for 15 days in each isotopically labeled media (CIL/Eurisotop), to ensure complete incorporation of isotopically labeled arginine and lysine (light label (R0K0, L) or semi-heavy label l-lysine-2HCl (2H4, 96–98%)/l-arginine-HCl (13C6, 99%) (R6K4, M) or l-lysine-2HCl (13C6, 99%; 15N2, 99%)/l-arginine-HCl (13C6, 99%; 15N4, 99%) heavy label (R10K8, H) (percentages represent the isotopic purity of the labeled amino acids). Eight 15-cm diameter plates were used per SILAC condition. Cells were rinsed with PBS, trypsinized, cryogrinded (56) and powder was resuspended in HNT lysis buffer (20 mM HEPES, pH 7.4, 150 mM NaCl, 0.5% triton X-100, protease inhibitor cocktail (cOmplete, Roche). Extracts were incubated 20 min at 4°C and clarified by centrifugation for 10 min at 20,000 *x g*. Extracts were pre-cleared by incubation with Protein G Sepharose beads (GE healthcare) for 1 h at 4°C. The control was extracted from the SILAC light condition prepared from parental HeLa cells that did not express the GFP fusion. Each extract was then incubated with 50 µL of GFP-Trap beads (Chromotek) for 1.5 h at 4°C, washed 5 times with HNT buffer, and beads from the different isotopic conditions were finally pooled. Bound proteins were eluted by adding 1% SDS to the beads and boiling for 10 min. Proteomic analysis was performed as previously described (19).

Label-free quantitative proteomic analysis of immunopurified extracts

For label-free proteomic analysis, IP was done in triplicate for each bait and eight 15-cm diameter plates were used per IP. Control IPs were performed in triplicates in parental HeLa cells devoid of GFP and used to normalize the IPs. Samples were electrophoresed onto 4% SDS-PAGE (stacking) and stained with colloidal Coomassie Brilliant Blue. Gel bands were reduced 1 h at 60°C by adding DiThioThreitol (DTT) to a final concentration of 10 mM and alkylated 20 min in the dark by adding iodoacetamide to a final concentration of 30 mM. An overnight digestion at 37°C was performed by adding trypsin (ratio enzyme:proteins of 1:50 [w]:[w]). Tryptic peptides were extracted using 80% acetonitrile (ACN)/0.1% formic acid (FA) in water. After solvent evaporation, samples were diluted with 0.1% FA prior to mass spectrometry analysis.

NanoLC-MS/MS analyses of the tryptic peptides were performed on a nanoACQUITY Ultra-Performance-LC-system (Waters, Milford, MA) coupled to a Q-Exactive plus Orbitrap mass spectrometer (ThermoFischer Scientific, Bremen, Germany). Samples were loaded on a Symmetry C18 precolumn (20 x 0.18 mm, 5 µm particle size, Waters Corp.). The peptides were separated on an ACQUITY UPLC® BEH130 C18 column (250 mm x 75 µm, 1.7 µm particle size, Waters Corp.). The solvent system consisted of 0.1% FA in water (solvent A) and 0.1% FA in ACN (solvent B). The samples were loaded into the enrichment column during 5 min at 5 µL/min with 99% of solvent A and 1% of solvent B. Elution of the peptides was performed at a flow rate of 450 nL/min with the following gradient: from 1 to 9.6% of solvent B in 27 min, 9.6-24% in 116 min and 24-32% of solvent B in 7 min.

The mass spectrometer source was operated at a spray voltage of 1.8 kV at 250°C. The system was operated in Data-Dependent-Acquisition (DDA) mode with automatic switching

between MS (AGC target $1e^6$ and maximum IT 200 ms on m/z range [400-1600] with R = 70,000) and MS/MS (AGC target $1e^5$ and maximum IT 50 ms on m/z range [200-2000] with R = 17,500) modes. The ten most abundant peptides (intensity threshold 2.10^4), preferably doubly and triply charged ions, were selected on each MS spectrum for further isolation and HCD fragmentation. The dynamic exclusion time was set to 30 s.

The raw data obtained during nanoLC-MS/MS analyses were interpreted using MaxQuant (version 1.5.8.3). The database used was extracted from UniProtKB on 14th March 2016 (human taxonomy 9606). Trypsin/P was selected as cleavage enzyme and a maximum of two missed cleavages was allowed. For MS/MS parameters, a parent mass tolerance of 5 ppm and a fragment mass tolerance of 0.05 Da were used. One fixed modification was taken into account: carbamidomethyl (Cys) and several variable modifications: oxidation (Met) and acetyl (protein N-term). For protein identification, false discovery rates were set to 1% for both peptide and protein levels. For the protein intensity of PIH1D1 in the three IP, we considered two peptides common to the three baits and showed values for the sum of intensities of these two peptides.

For other protein quantification, the "match between runs" option was enabled and only unmodified peptides were used. MaxLFQ quantification was applied using a minimal ratio count of one unique peptide. All other MaxQuant parameters were set as default. The ProteinGroups.txt file was used for statistical processing after removal of contaminants, reverse and proteins only identified by site.

Phosphoproteomic analysis

Tryptic peptides were obtained as described for the label-free quantitative proteomic analysis. Ten micrograms were saved for injection of the total extract and 230 µg were used for the titanium dioxide (TiO_2) enrichment. TiO_2 beads (Titansphere TiO_2 5 µm GL SCIENCE INC. #5020-75000, Interchim) were resuspended (6 mg of beads in 1 mL of buffer) in binding buffer containing 80% ACN, 5% trifluoroacetic acid (TFA) and 1 M glycolic acid. After 5 min of equilibration, TiO_2 slurry was distributed in eppendorf tubes (2.4 mg of TiO_2 for 100 µg of peptides) and the supernatant was eliminated by centrifugation (1 min at 1,600 *x g*). Samples were resuspended in the binding buffer at a concentration of 0.5 µg/µL. After transferring the samples into the TiO_2 beads, the supernatant was removed after 15 min of incubation at RT. Beads were wash with binding buffer (400 µL, 5 min), then with a solution of 80% ACN, 0.1% TFA (400 µL, 1 min) and finally with 10% ACN, 0.2% TFA (400 µL, 1 min). Beads were dried and phosphopeptides were eluted with 150 µL of 1% NH_4OH pH 11.3. Ten microliters of TFA were used to acidify samples for desalting. R3 resin (Oligo-R3 bulk media. #1-1339-03, Thermo) was resuspended in ACN (20 mg of beads with 800 µL of solvent) and 40 µL of R3 slurry was pack in a GELoader tip (0.5-20 µL, 62 mm, # 0030001222, Eppendorf) previously flattened. After equilibration of the resin with 20 µL of water containing 0.1% FA, sample was loaded and passed through by applying air pressure using a plastic syringe. Sample was washed with 20 µL of acidified water and phosphopeptides were eluted with 40 µL of 80% ACN, 0.1% FA.

The nanoLC-MS/MS analyses of total extracts and phosphospeptide fractions were acquired and interpreted as previously described by adding phosphorylation (Ser, Thr, Tyr) as variable modifications. Phosphopeptides were validated with a localization probability equal to or greater than 75%.

Co-expression assays

The pnEA::TSC1_D4b (726-1047) and pnCS::PIH1D1_NTER (1-180) constructs were co-transformed into *E. coli* BL21(DE3) competent cells supplemented with the pRARE2 plasmid.

For the binding control to the cobalt resin (TALON, TaKaRa), the pnCS construct alone was transformed into BL21(DE3)pRARE2 competent cells. Clones were selected on LB-agar plates containing the appropriate antibiotics, grown into 100 mL LB medium at 37°C until the absorbance at 600 nm reaches 0.7, then the expression was induced by addition of 0.1 mM IPTG (isopropyl β-D-1-thiogalactopyranoside), and after 16 to 18 h culture at 20°C, cells were harvested. The cell pellet was resuspended into lysis buffer (HEPES 25 mM pH 7.5; NaCl 300 mM; Imidazole 10 mM; TCEP 0.5 mM), sonicated and centrifuged 30 min at 16,000 *x g*. Then cobalt resin was added to the soluble fraction and after 30 min incubation, resin was washed 3 times with lysis buffer to remove any non-specific binding, and the proteins of interest were eluted from the resin with lysis buffer supplemented with 300 mM imidazole. The purification result was analyzed after SDS-PAGE (Poly Acrylamide Gel Electrophoresis) and Coomassie blue staining.

HIS-Avi-TSC1(725-1047) was co-expressed together with HIS-RuvBL1 (R1), RuvBL2-Fh8-FLAG (R2) and BirA in E. coli Tuner cells. PB medium was used to grow the bacteria, and expression of all constructs was induced by supplementing with 500 µM of IPTG once the cultures reached an optical density (OD600) of 1.8. BirA specifically biotinylates the Avi-tag; therefore, to provide sufficient concentrations of biotin, 2 mg/mL was added to the bacteria during the induction of protein expression. Construct expression was performed at 18 °C for 16h.

During a 10 min centrifugation at 8,000 rpm in a Beckman Avanti J-26 with a JA-10 rotor, cells were harvested and subsequently resuspended in lysis buffer (25 mM HEPES pH 8.0, 200 mM NaCl, 2 mM MgCl2, 15 mM Imidazole, 0.5 mM TCEP, 10% Glycerol, supplemented with cOmplete protease inhibitor cocktail and Benzonase). Cells were lysed by applying 18 kPsi per shot in a multi-cycle cell disruptor. To separate soluble from insoluble fractions, the lysates were centrifuged in a Beckman Avanti J-26 with a JA-14 rotor at 13,000 rpm. The soluble fraction was filtered through a 0.45 µm pore filter before injecting it to a Cytiva HisTrap HP prepacked column capturing the His-tagged R1 as well as the His-tagged TSC1(725-1047). To increase the contact time between resin and soluble cell lysate, the injection was performed overnight.

Washing the beads using the lysis buffer ensured removal of unspecific bound proteins from the HisTrap column. Bound proteins were eluted by applying a 10x bed-volume (50 mL) gradient from lysis buffer to elution buffer (25 mM HEPES pH 8.0, 200 mM NaCl, 2 mM MgCl2, 1 M Imidazole, 0.5 mM TCEP, 10% Glycerol). Elution of bound proteins was followed by monitoring the absorbance at 280 nm (A280 nm) and the collected fractions containing protein were analyzed by SDS-PAGE followed by Coomassie staining, as well as by Western blots against biotinylated Avi-tag only carried by TSC1(725-1047). Fractions showing the co-elution of all three proteins, were pooled and loaded to 500 µL of anti-Flag M2 affinity gel capturing the Flag-tagged R2. The anti-Flag affinity gel was washed (25 mM HEPES pH 8.0, 200 mM NaCl, 2 mM $MgCl_2$, 0.5 mM TCEP, 10% Glycerol)) with 30 times the bed volume before bound proteins were eluted by supplementing the buffer with 200 µg/mL of the Merck Flag-peptide. Eluted proteins were analyzed by SDS-PAGE followed by Coomassie staining, as well as by Western blots against His-tag (TSC1(725-1047) and R1), Flag-tag (R2), and biotinylated Avi-tag (TSC1(725-1047)).

Yeast two-hybrid assay

Plasmids pACTII and pAS2ΔΔ were introduced into haploid *Saccharomyces cerevisiae* strains (Y187 and CG1945, respectively). Strains were crossed and grown on YEPD medium and then plated on double (–Leu–Trp) and triple selective media (–Leu–Trp–His). Growth was assessed visually after 3 days at 30°C. The strength of interactions was evaluated by comparing the number of clones growing on –Leu–Trp (selection of diploids) and –Leu–Trp–His plates (selection for interaction).

Cytometry for cell cycle analysis

Cells were collected by trypsinization and resuspend in medium containing serum to inactivate trypsin. Then, cells were centrifuged at 200 *x g* for 6 min at RT. Supernatant was removed and cells resuspended in 1 mL of cold PBS. As gently vortexing cells, 9 mL of 70% cold ethanol was added in a polypropylene falcon tube. Cells were then stored at 4°C for at least 2 h before being centrifuged 10 min at 200 *x g* at 4°C. Pellet was resuspend in 3 mL of cold PBS and centrifuge again 10 min at 200 *x g* at 4°C. Pellet was resuspend in 500 µL of Propidium Iodide (PI)/Triton 100X staining solution. Cells were incubated at 37°C for 15 min before to come back on ice and being protected from light. Data were acquired on Novocyte flow cytometer with a 488 nm excitation laser and analysis was done with NovoExpress.

Data availability

Mass spectrometry data have been deposited to the Pride database. The assigned identifier for label free proteomics of PIH1D1, PIH1D1_NTER and PIH1D1_NTER_K64A IPs (Table S1) is PXD032335. The assigned identifier for phospho-proteomics of PIH1D1 and PIH1D1_NTER IPs (Table S2) is PXD032331. The assigned identifier for SILAC IP GFP-TSC2 (Table S3) is PXD030402.

Supplemental data

This article contains supplemental data. Figure S1 to S5 and Table S1 to S3.

Table S1 : Difference in the proteomic analysis of PIH1D1 with PIH1D1_NTER and PIH1D1_NTER with PIH1D1_NTER_K64A IP

Table S2 : Hit list of the phospho-proteomic analysis of PIH1D1 and PIH1D1_NTER IP

Table S3 : Hit list of the GFP-TSC2 SILAC IP. Significance B is calculated according to (57)

Acknowledgment

This work was supported by grants from Centre National de la Recherche Scientifique (CNRS); Université de Montpellier (UM); Université de Lorraine (UL); the Agence Nationale de la Recherche [ANR-16-CE11-0032-04]; grants from the Ligue Nationale Contre le Cancer ('équipe labellisée'); Institut national du Cancer [INCa PLBio 2016-161]; Fundação para a Ciência e Tecnologia/Ministério da Ciência, Tecnologia e Ensino Superior (FCT/MCTES, Portugal) through national funds to iNOVA4Health (UIDB/ 04462/ 2020, UIDP/04462/2020) and the Associate Laboratory LS4FUT URE (LA/P/0087/2020). CA was supported by La ligue Contre le Cancer and Fondation pour la Recherche Médicale. Mass spectrometry for SILAC-IP experiments was carried out using the facilities of the Montpellier Proteomics Platform (PPM, BioCampus Montpellier). We also thank MRI and MGC facilities of UMS Montpellier BioCampus. We thank C. Goujon for the gift of HEK 293T cells expressing Cas9 and Y. Abel for cloning of PIH1D1 KO cells. We thank B. Pradet-Balade, D. Helmlinger and P. Marin for their discussion on the project and M. Hourques and D. Soumayla Seyni for their help in Y2H and IP LUMIER assays. We also thank S. Boulon for reading of the manuscript.

Author contributions

C. Abéza performed all experiments shown in Figs 1, 2, 3C,5,6 and 7. M-E. Chagot performed experiment shown in Fig 4A and P. Busse and A. C.F. Paiva in Fig 4B. M-C. Robert prepared the KO cell lines. F.Vandermoere analyzed proteomic data of Fig 6B and J. Schneider and C. Schaeffer proteomic data of Fig 1 and 3A. C. Abéza and C. Verheggen prepared all the figures. C. Verheggen, E. Bertrand, B. Charpentier, P. Sousa, T. Bandeiras, X. Manival, S. Cianferani supervised the project. C. Verheggen and E. Bertrand designed the experiments and wrote the manuscript.

Conflict of interest

The authors declare that they have no conflicts of interest with the contents of this article.

Abbeviations

KO knock out

IP immunoprecipitation

HSP heat shock protein

HRP horseradish peroxidase

FFL firefly luciferase

LUMIER luminescence-based mammalian interactome mapping

MS mass spectrometry

PBS phosphate buffer saline

PIKK phosphatidylinositol 3-kinase-related kinase

RL renilla luciferase

R2TP Rvb1/Rvb2/Tah1/Pih1 complex in yeast and RUVBL1/RUVBL2/RPAP3/PIH1D1 in human

RT room temperature

RUVBL1/2 RUVBL1/RUVBL2 complex

TPR tetratricopeptide

TSC tuberous sclerosis complex

SILAC stable isotope labeling using amino acids in cell culture

References

1. Schopf, F. H., Biebl, M. M., and Buchner, J. (2017) The HSP90 chaperone machinery. *Nat Rev Mol Cell Biol*. **18**, 345–360.

2. Luengo, T. M., Mayer, M. P., and Rüdiger, S. G. D. (2019) The Hsp70–Hsp90 Chaperone Cascade in Protein Folding. *Trends in Cell Biology*. **29**, 164–177.

3. Maiti, S., and Picard, D. (2022) Cytosolic Hsp90 Isoform-Specific Functions and Clinical Significance. *Biomolecules*. **12**, 1166.

4. Hoter, A., El-Sabban, M. E., and Naim, H. Y. (2018) The HSP90 Family: Structure, Regulation, Function, and Implications in Health and Disease. *International Journal of Molecular Sciences*. **19**, 2560.

5. Taipale, M., Tucker, G., Peng, J., Krykbaeva, I., Lin, Z.-Y., Larsen, B., Choi, H., Berger, B., Gingras, A.-C., and Lindquist, S. (2014) A quantitative chaperone interaction network reveals the architecture of cellular protein homeostasis pathways. *Cell*. **158**, 434–448.

6. Seraphim, T. V., Nano, N., Cheung, Y. W. S., Aluksanasuwan, S., Colleti, C., Mao, Y.-Q., Bhandari, V., Young, G., Höll, L., Phanse, S., Gordiyenko, Y., Southworth, D. R., Robinson, C. V., Thongboonkerd, V., Gava, L. M., Borges, J. C., Babu, M., Barbosa, L. R. S., Ramos, C. H. I., Kukura, P., and Houry, W. A. (2021) Assembly principles of the human R2TP chaperone complex reveal the presence of R2T and R2P complexes. *Structure*. 10.1016/j.str.2021.08.002.

7. Muñoz-Hernández, H., Pal, M., Rodríguez, C. F., Fernandez-Leiro, R., Prodromou, C., Pearl, L. H., and Llorca, O. (2019) Structural mechanism for regulation of the AAA-ATPases RUVBL1-RUVBL2 in the R2TP co-chaperone revealed by cryo-EM. *Sci Adv*. **5**, eaaw1616

8. Lynham, J., and Houry, W. A. (2022) The Role of Hsp90-R2TP in Macromolecular Complex Assembly and Stabilization. *Biomolecules*. **12**, 1045.

9. Dauden, M. I., López-Perrote, A., and Llorca, O. (2021) RUVBL1–RUVBL2 AAA-ATPase: a versatile scaffold for multiple complexes and functions. *Current Opinion in Structural Biology*. **67**, 78–85.

10. Houry, W. A., Bertrand, E., and Coulombe, B. (2018) The PAQosome, an R2TP-Based Chaperone for Quaternary Structure Formation. *Trends in Biochemical Sciences*. **43**, 4–9.

11. Bizarro, J., Charron, C., Boulon, S., Westman, B., Pradet-Balade, B., Vandermoere, F., Chagot, M.-E., Hallais, M., Ahmad, Y., Leonhardt, H., Lamond, A., Manival, X., Branlant, C., Charpentier, B., Verheggen, C., and Bertrand, E. (2014) Proteomic and 3D structure analyses highlight the C/D box snoRNP assembly mechanism and its control. *J Cell Biol*. **207**, 463–480.

12. Bizarro, J., Dodré, M., Huttin, A., Charpentier, B., Schlotter, F., Branlant, C., Verheggen, C., Massenet, S., and Bertrand, E. (2015) NUFIP and the HSP90/R2TP chaperone bind the SMN complex and facilitate assembly of U4-specific proteins. *Nucleic Acids Res*. **43**,

8973–8989.

13. Cloutier, P., Poitras, C., Durand, M., Hekmat, O., Fiola-Masson, É., Bouchard, A., Faubert, D., Chabot, B., and Coulombe, B. (2017) R2TP/Prefoldin-like component RUVBL1/RUVBL2 directly interacts with ZNHIT2 to regulate assembly of U5 small nuclear ribonucleoprotein. *Nat Commun*. **8**, 15615.

14. Machado-Pinilla, R., Liger, D., Leulliot, N., and Meier, U. T. (2012) Mechanism of the AAA+ ATPases pontin and reptin in the biogenesis of H/ACA RNPs. *RNA*. **18**, 1833–1845.

15. Malinová, A., Cvačková, Z., Matějů, D., Hořejší, Z., Abéza, C., Vandermoere, F., Bertrand, E., Staněk, D., and Verheggen, C. (2017) Assembly of the U5 snRNP component PRPF8 is controlled by the HSP90/R2TP chaperones. *Journal of Cell Biology*. **216**, 1579–1596.

16. Boulon, S., Pradet-Balade, B., Verheggen, C., Molle, D., Boireau, S., Georgieva, M., Azzag, K., Robert, M.-C., Ahmad, Y., Neel, H., Lamond, A. I., and Bertrand, E. (2010) HSP90 and its R2TP/Prefoldin-like cochaperone are involved in the cytoplasmic assembly of RNA polymerase II. *Mol Cell*. **39**, 912–924.

17. Martino, F., Pal, M., Muñoz-Hernández, H., Rodríguez, C. F., Núñez-Ramírez, R., Gil-Carton, D., Degliesposti, G., Skehel, J. M., Roe, S. M., Prodromou, C., Pearl, L. H., and Llorca, O. (2018) RPAP3 provides a flexible scaffold for coupling HSP90 to the human R2TP co-chaperone complex. *Nat Commun*. **9**, 1501.

18. Dos Santos Morais, R., Santo, PE., Ley, M., Schelcher, C., Abel, Y., Plassart, L., Deslignière, E., Chagot, ME., Quinternet, M., Paiva, ACF., Hessmann, S., Morellet, N.M.F., Sousa, P., Vandermoere, F., Bertrand, E., Charpentier, B., Bandeiras, TM., Plisson-Chastang, C., Verheggen, C., Cianférani, S., Manival, X. (2022) Deciphering cellular and molecular determinants of human DPCD protein in complex with RUVBL1/RUVBL2 AAA-ATPases. *J Mol Biol.* **434**, 167760.

19. Maurizy, C., Quinternet, M., Abel, Y., Verheggen, C., Santo, P. E., Bourguet, M., C F Paiva, A., Bragantini, B., Chagot, M.-E., Robert, M.-C., Abeza, C., Fabre, P., Fort, P., Vandermoere, F., M F Sousa, P., Rain, J.-C., Charpentier, B., Cianférani, S., Bandeiras, T. M., Pradet-Balade, B., Manival, X., and Bertrand, E. (2018) The RPAP3-Cterminal domain identifies R2TP-like quaternary chaperones. *Nat Commun*. **9**, 2093.

20. Henri, J., Chagot, M.-E., Bourguet, M., Abel, Y., Terral, G., Maurizy, C., Aigueperse, C., Georgescauld, F., Vandermoere, F., Saint-Fort, R., Behm-Ansmant, I., Charpentier, B., Pradet-Balade, B., Verheggen, C., Bertrand, E., Meyer, P., Cianférani, S., Manival, X., and Quinternet, M. (2018) Deep Structural Analysis of RPAP3 and PIH1D1, Two Components of the HSP90 Co-chaperone R2TP Complex. *Structure*. **26**, 1196-1209.e8

21. Pal, M., Morgan, M., Phelps, S. E. L., Roe, S. M., Parry-Morris, S., Downs, J. A., Polier, S., Pearl, L. H., and Prodromou, C. (2014) Structural Basis for Phosphorylation-Dependent Recruitment of Tel2 to Hsp90 by Pih1. *Structure*. **22**, 805–818.

22. Boulon, S., Marmier-Gourrier, N., Pradet-Balade, B., Wurth, L., Verheggen, C., Jády, B. E., Rothé, B., Pescia, C., Robert, M.-C., Kiss, T., Bardoni, B., Krol, A., Branlant, C., Allmang, C., Bertrand, E., and Charpentier, B. (2008) The Hsp90 chaperone controls the biogenesis of L7Ae RNPs through conserved machinery. *J Cell Biol*. **180**, 579–595.

23. Serna, M., González-Corpas, A., Cabezudo, S., López-Perrote, A., Degliesposti, G., Zarzuela, E., Skehel, J. M., Muñoz, J., and Llorca, O. (2022) CryoEM of RUVBL1–RUVBL2–ZNHIT2, a complex that interacts with pre-mRNA-processing-splicing factor 8. *Nucleic Acids Research*. **50**, 1128–1146.

24. Verheggen, C., Pradet-Balade, B., and Bertrand, E. (2015) SnoRNPs, ZNHIT proteins and the R2TP pathway. *Oncotarget*. **6**, 41399–41400.

25. Hořejší, Z., Stach, L., Flower, T. G., Joshi, D., Flynn, H., Skehel, J. M., O'Reilly, N. J., Ogrodowicz, R. W., Smerdon, S. J., and Boulton, S. J. (2014) Phosphorylation-Dependent PIH1D1 Interactions Define Substrate Specificity of the R2TP Cochaperone Complex. *Cell Reports*. **7**, 19–26.

26. Xu, R., Xu, Y., Huo, W., Lv, Z., Yuan, J., Ning, S., Wang, Q., Hou, M., Gao, G., Ji, J., Chen, J., Guo, R., and Xu, D. (2018) Mitosis-specific MRN complex promotes a mitotic signaling cascade to regulate spindle dynamics and chromosome segregation. *Proceedings of the National Academy of Sciences*. **115**, E10079–E10088.

27. von Morgen, P., Burdova, K., Flower, T. G., O'Reilly, N. J., Boulton, S. J., Smerdon, S. J., Macurek, L., and Hořejší, Z. (2017) MRE11 stability is regulated by CK2-dependent interaction with R2TP complex. *Oncogene*. **36**, 4943–4950.

28. von Morgen, P., Hořejší, Z., and Macurek, L. (2015) Substrate recognition and function of the R2TP complex in response to cellular stress. *Front Genet*. **6**, 69.

29. Abel, Y., Charron, C., Virciglio, C., Bourguignon-Igel, V., Quinternet, M., Chagot, M.-E., Robert, M.-C., Verheggen, C., Branlant, C., Bertrand, E., Manival, X., Charpentier, B., and Rederstorff, M. (2022) The interaction between RPAP3 and TRBP reveals a possible involvement of the HSP90/R2TP chaperone complex in the regulation of miRNA activity. *Nucleic Acids Res*. **50**, 2172–2189.

30. Guertin, D. A., and Sabatini, D. M. (2007) Defining the role of mTOR in cancer. *Cancer Cell*. **12**, 9–22.

31. Dodd, K. M., and Dunlop, E. A. (2016) Tuberous sclerosis—A model for tumour growth. *Seminars in Cell & Developmental Biology*. **52**, 3–11.

32. Zhang, H., Cicchetti, G., Onda, H., Koon, H. B., Asrican, K., Bajraszewski, N., Vazquez, F., Carpenter, C. L., and Kwiatkowski, D. J. (2003) Loss of Tsc1/Tsc2 activates mTOR and disrupts PI3K-Akt signaling through downregulation of PDGFR. *J Clin Invest*. **112**, 1223–1233.

33. Pai, G. M., Zielinski, A., Koalick, D., Ludwig, K., Wang, Z.-Q., Borgmann, K., Pospiech, H., and Rubio, I. (2016) TSC loss distorts DNA replication programme and sensitises cells to genotoxic stress. *Oncotarget*. **7**, 85365–85380.

34. Ramlaul, K., Fu, W., Li, H., de Martin Garrido, N., He, L., Trivedi, M., Cui, W., Aylett, C. H. S., and Wu, G. (2021) Architecture of the Tuberous Sclerosis Protein Complex. *J Mol Biol*. **433**, 166743.

35. Yang, H., Yu, Z., Chen, X., Li, J., Li, N., Cheng, J., Gao, N., Yuan, H.-X., Ye, D., Guan, K.-L., and Xu, Y. (2021) Structural insights into TSC complex assembly and GAP

activity on Rheb. *Nat Commun*. **12**, 339.

36. Fitzian, K., Brückner, A., Brohée, L., Zech, R., Antoni, C., Kiontke, S., Gasper, R., Matos, A. L. L., Beel, S., Wilhelm, S., Gerke, V., Ungermann, C., Nellist, M., Raunser, S., Demetriades, C., Oeckinghaus, A., and Kümmel, D. (2021) TSC1 binding to lysosomal PIPs is required for TSC complex translocation and mTORC1 regulation. *Molecular Cell*. **81**, 2705-2721.e8

37. Woodford, M. R., Sager, R. A., Marris, E., Dunn, D. M., Blanden, A. R., Murphy, R. L., Rensing, N., Shapiro, O., Panaretou, B., Prodromou, C., Loh, S. N., Gutmann, D. H., Bourboulia, D., Bratslavsky, G., Wong, M., and Mollapour, M. (2017) Tumor suppressor Tsc1 is a new Hsp90 co-chaperone that facilitates folding of kinase and non-kinase clients. *EMBO J*. **36**, 3650–3665.

38. Backe, S. J., Sager, R. A., Meluni, K. A., Woodford, M. R., Bourboulia, D., and Mollapour, M. (2022) Emerging Link between Tsc1 and FNIP Co-Chaperones of Hsp90 and Cancer. *Biomolecules*. **12**, 928.

39. Hořejší, Z., Takai, H., Adelman, C. A., Collis, S. J., Flynn, H., Maslen, S., Skehel, J. M., Lange, T. de, and Boulton, S. J. (2010) CK2 Phospho-Dependent Binding of R2TP Complex to TEL2 Is Essential for mTOR and SMG1 Stability. *Molecular Cell*. **39**, 839–850.

40. Barrios-Rodiles, M., Brown, K. R., Ozdamar, B., Bose, R., Liu, Z., Donovan, R. S., Shinjo, F., Liu, Y., Dembowy, J., Taylor, I. W., Luga, V., Przulj, N., Robinson, M., Suzuki, H., Hayashizaki, Y., Jurisica, I., and Wrana, J. L. (2005) High-throughput mapping of a dynamic signaling network in mammalian cells. *Science*. **307**, 1621–1625.

41. Mozaffari, M., Hoogeveen-Westerveld, M., Kwiatkowski, D., Sampson, J., Ekong, R., Povey, S., den Dunnen, J. T., van den Ouweland, A., Halley, D., and Nellist, M. (2009) Identification of a region required for TSC1 stability by functional analysis of TSC1 missense mutations found in individuals with tuberous sclerosis complex. *BMC Med Genet*. **10**, 88.

42. Santiago Lima, A. J., Hoogeveen-Westerveld, M., Nakashima, A., Maat-Kievit, A., van den Ouweland, A., Halley, D., Kikkawa, U., and Nellist, M. (2014) Identification of regions critical for the integrity of the TSC1-TSC2-TBC1D7 complex. *PLoS One*. **9**, e93940.

43. Hodges, A. K., Li, S., Maynard, J., Parry, L., Braverman, R., Cheadle, J. P., DeClue, J. E., and Sampson, J. R. (2001) Pathological mutations in TSC1 and TSC2 disrupt the interaction between hamartin and tuberin. *Hum Mol Genet*. **10**, 2899–2905.

44. Hoogeveen-Westerveld, M., Exalto, C., Maat-Kievit, A., van den Ouweland, A., Halley, D., and Nellist, M. (2010) Analysis of TSC1 truncations defines regions involved in TSC1 stability, aggregation and interaction. *Biochimica et Biophysica Acta (BBA) - Molecular Basis of Disease*. **1802**, 774–781.

45. Gai, Z., Chu, W., Deng, W., Li, W., Li, H., He, A., Nellist, M., and Wu, G. (2016) Structure of the TBC1D7-TSC1 complex reveals that TBC1D7 stabilizes dimerization of the TSC1 C-terminal coiled coil region. *J Mol Cell Biol*. **8**, 411–425.

46. Assimon, V. A., Tang, Y., Vargas, J. D., Lee, G. J., Wu, Z. Y., Lou, K., Yao, B., Menon, M.-K., Pios, A., Perez, K. C., Madriaga, A., Buchowiecki, P. K., Rolfe, M., Shawver, L., Jiao, X., Le Moigne, R., Zhou, H.-J., and Anderson, D. J. (2019) CB-6644 Is a Selective

Inhibitor of the RUVBL1/2 Complex with Anticancer Activity. *ACS Chem Biol*. **14**, 236–244.

47. Qin, J., Wang, Z., Hoogeveen-Westerveld, M., Shen, G., Gong, W., Nellist, M., and Xu, W. (2016) Structural Basis of the Interaction between Tuberous Sclerosis Complex 1 (TSC1) and Tre2-Bub2-Cdc16 Domain Family Member 7 (TBC1D7). *J Biol Chem*. **291**, 8591–8601.

48. Zech, R., Kiontke, S., Mueller, U., Oeckinghaus, A., and Kümmel, D. (2016) Structure of the Tuberous Sclerosis Complex 2 (TSC2) N Terminus Provides Insight into Complex Assembly and Tuberous Sclerosis Pathogenesis *. *Journal of Biological Chemistry*. **291**, 20008–20020.

49. Lee, D.-F., Kuo, H.-P., Chen, C.-T., Hsu, J.-M., Chou, C.-K., Wei, Y., Sun, H.-L., Li, L.-Y., Ping, B., Huang, W.-C., He, X., Hung, J.-Y., Lai, C.-C., Ding, Q., Su, J.-L., Yang, J.-Y., Sahin, A. A., Hortobagyi, G. N., Tsai, F.-J., Tsai, C.-H., and Hung, M.-C. (2007) IKK beta suppression of TSC1 links inflammation and tumor angiogenesis via the mTOR pathway. *Cell*. **130**, 440–455.

50. Ma, L., Chen, Z., Erdjument-Bromage, H., Tempst, P., and Pandolfi, P. P. (2005) Phosphorylation and functional inactivation of TSC2 by Erk implications for tuberous sclerosis and cancer pathogenesis. *Cell*. **121**, 179–193.

51. Dibble, C. C., and Cantley, L. C. (2015) Regulation of mTORC1 by PI3K signaling. *Trends in Cell Biology*. **25**, 545–555.

52. Trepel, J., Mollapour, M., Giaccone, G., and Neckers, L. (2010) Targeting the dynamic HSP90 complex in cancer. *Nat Rev Cancer*. **10**, 537–549.

53. Neckers, L., and Workman, P. (2012) Hsp90 molecular chaperone inhibitors: are we there yet? *Clin Cancer Res*. **18**, 64–76.

54. Maurizy, C., Abeza, C., Lemmers, B., Gabola, M., Longobardi, C., Pinet, V., Ferrand, M., Paul, C., Bremond, J., Langa, F., Gerbe, F., Jay, P., Verheggen, C., Tinari, N., Helmlinger, D., Lattanzio, R., Bertrand, E., Hahne, M., and Pradet-Balade, B. (2021) The HSP90/R2TP assembly chaperone promotes cell proliferation in the intestinal epithelium. *Nat Commun*. **12**, 4810.

55. Tantale, K., Mueller, F., Kozulic-Pirher, A., Lesne, A., Victor, J.-M., Robert, M.-C., Capozi, S., Chouaib, R., Bäcker, V., Mateos-Langerak, J., Darzacq, X., Zimmer, C., Basyuk, E., and Bertrand, E. (2016) A single-molecule view of transcription reveals convoys of RNA polymerases and multi-scale bursting. *Nat Commun*. **7**, 12248.

56. Domanski, M., Molloy, K., Jiang, H., Chait, B. T., Rout, M. P., Jensen, T. H., and LaCava, J. (2012) Improved methodology for the affinity isolation of human protein complexes expressed at near endogenous levels. *Biotechniques*. **0**, 1–6.

57. Cox, J., and Mann, M. (2008). MaxQuant enables high peptide identification rates, individualized p.p.b.-range mass accuracies and proteome-wide protein quantification. *Nat Biotechnol* **26**, 1367–1372.

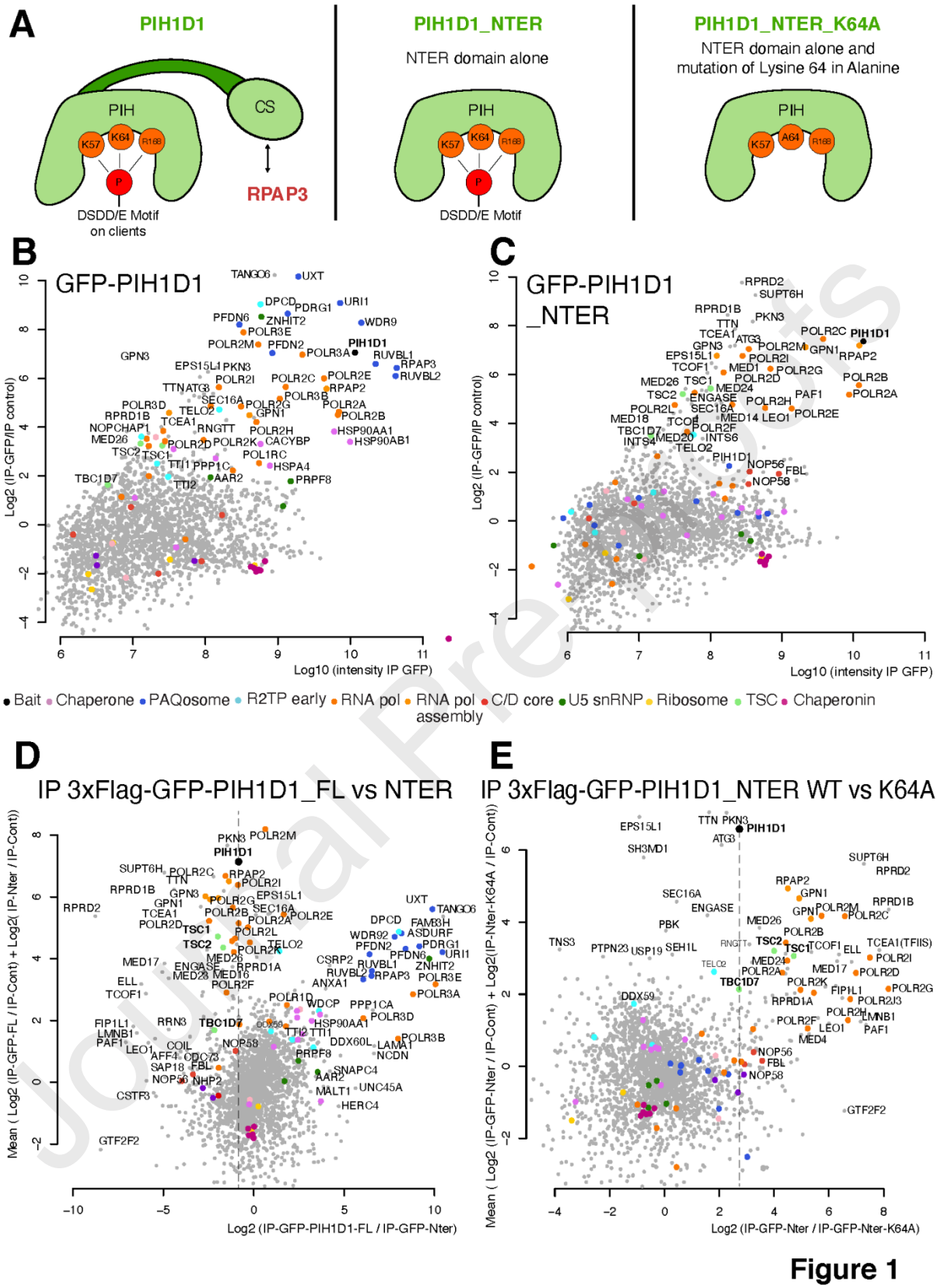
A
PIH1D1
PIH
CS
K57
K64
R188
P
RPAP3
DSDD/E Motif
on clients
PIH1D1_NTER
NTER domain alone
PIH
K57
K64
R188
P
DSDD/E Motif
PIH1D1_NTER_K64A
NTER domain alone and
mutation of Lysine 64 in Alanine
PIH
K57
A64
R188
B
GFP-PIH1D1
Log2 (IP-GFP/IP control)
Log10 (intensity IP GFP)
C
GFP-PIH1D1
_NTER
Log2 (IP-GFP/IP control)
Log10 (intensity IP GFP)
Bait
Chaperone
PAQosome
R2TP early
RNA pol
RNA pol assembly
C/D core
U5 snRNP
Ribosome
TSC
Chaperonin
D
IP 3xFlag-GFP-PIH1D1_FL vs NTER
Mean (Log2 (IP-GFP-FL / IP-Cont) + Log2(IP-Nter / IP-Cont))
Log2 (IP-GFP-PIH1D1-FL / IP-GFP-Nter)
E
IP 3xFlag-GFP-PIH1D1_NTER WT vs K64A
Mean (Log2 (IP-GFP-Nter / IP-Cont) + Log2(IP-Nter-K64A / IP-Cont))
Log2 (IP-GFP-Nter / IP-GFP-Nter-K64A)

Figure 1

Figure 1. Label-free proteomic analyses of GFP-PIH1D1, GFP-PIH1D1_NTER and GFP-PIH1D1_NTER_K64A IP partners.

(A) Schematic representation of the human PIH1D1 structural domains showing the interaction of PH1D1_NTER domain with a consensus motif found in some of its binding partners. PIH1D1 full length (left), as well as wild-type and mutant PIH1D1_NTER (middle and right), were used as baits for label-free proteomic studies after IP. **(B,C)** Label-free proteomic analyses after IP of GFP-PIH1D1, GFP-PIH1D1_NTER. Control IP was done in parental HeLa cells. The graphs display the enrichment over the control (Log2 (IP/Ct; y axis) as a function of LFQ intensity in the IP (Log10 (intensity IP GFP); x axis). Each dot is a protein and the color code is indicated below the graph. **(D,E)** The graphs display the difference between GFP-PIH1D1 IP and GFP-PIH1D1_NTER IP (D) and between GFP-PIH1D1_NTER IP and GFP-PIH1D1_NTER_K64A IP (E).

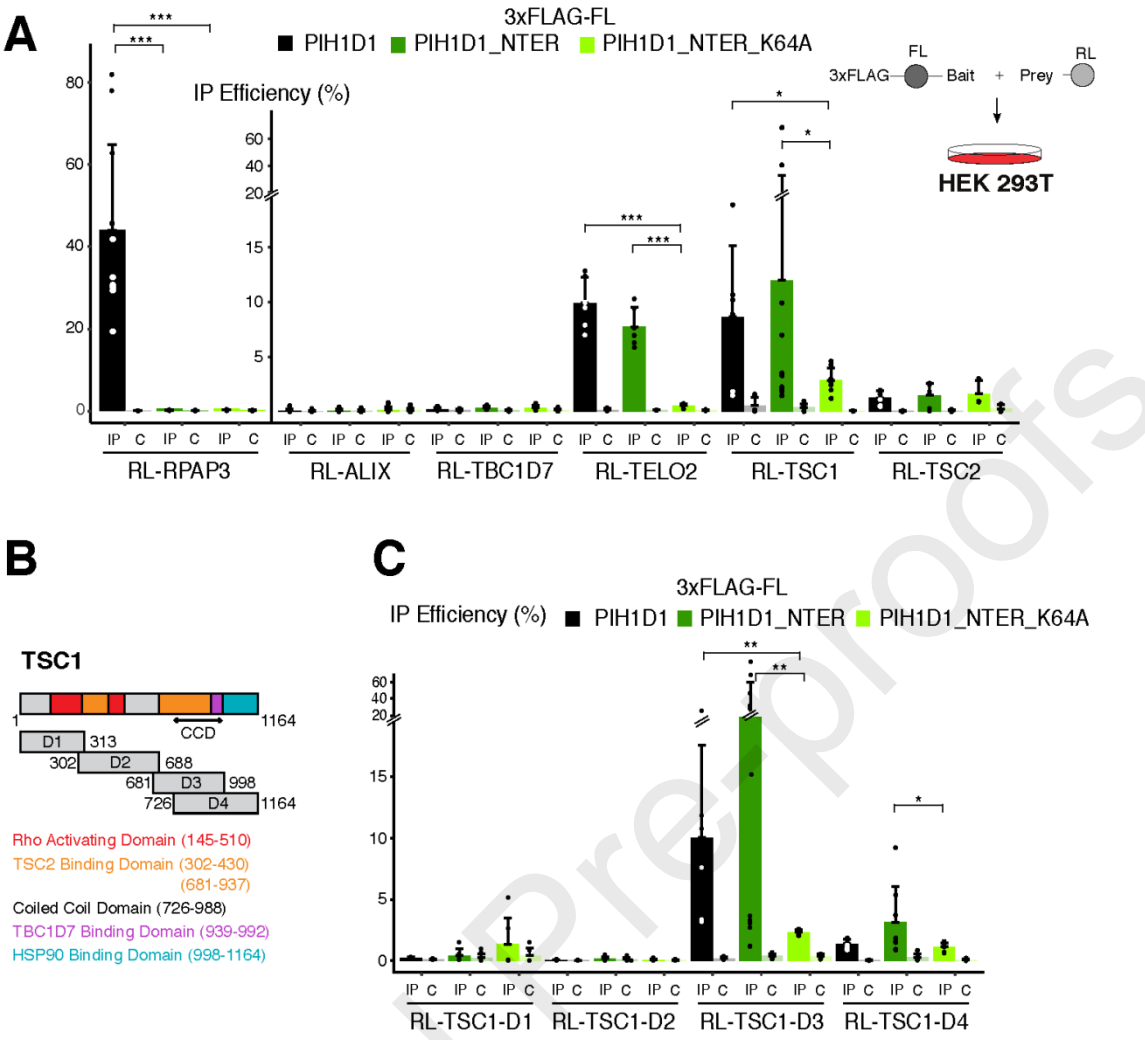

Figure 2

Figure 2. Differential interaction of TSC1 with PIH1D1, PIH1D1_NTER and PIH1D1_NTER_K64A.

(A) LUMIER IP showing *in vivo* interaction between PIH1D1, PIH1D1_NTER and PIH1D1_NTER_K64A fused to 3XFLAG-FL and TSC complex subunits fused to RL. TEL2 and ALIX fused to RL were used as positive and negative controls respectively. HEK 293T cells were co-transfected with a plasmid coding for the bait (color code indicated on the top of the graph) and a plasmid coding for the prey (indicated below the graph). Anti-FLAG IP is performed after 48 h. The graph plots the IP efficiency (%). It measures the co-precipitation of the RL fusion proteins (RL IP/Input), normalized by the amount of FL fusion immunoprecipitated (FL IP/Input). C is the IP efficiency with the same extract but in a control well without antibody. Bars represent the means. Experiments were repeated 4 or 5 times and each experiment itself contained two replicates. Error bars: standard deviation. Stars: values significantly different with *** = p-value < 0.001; ** = p- value < 0.01; * = p-value < 0.05 (Student t-test). **(B)** Schematic architecture of human TSC1. Known domains of TSC1 described from the literature are represented with different colors and named below the drawing. CCD is for Coiled-Coil domain. Truncated mutants D1-D4 were generated that contains these different domains (numbering corresponds to amino-acids). **(C)** LUMIER IP showing *in vivo* interaction between PIH1D1, PIH1D1_NTER, PH1D1_NTER_K64A fused to 3XFLAG-FL and TSC1 truncated mutants fused to RL. Legend as in A.

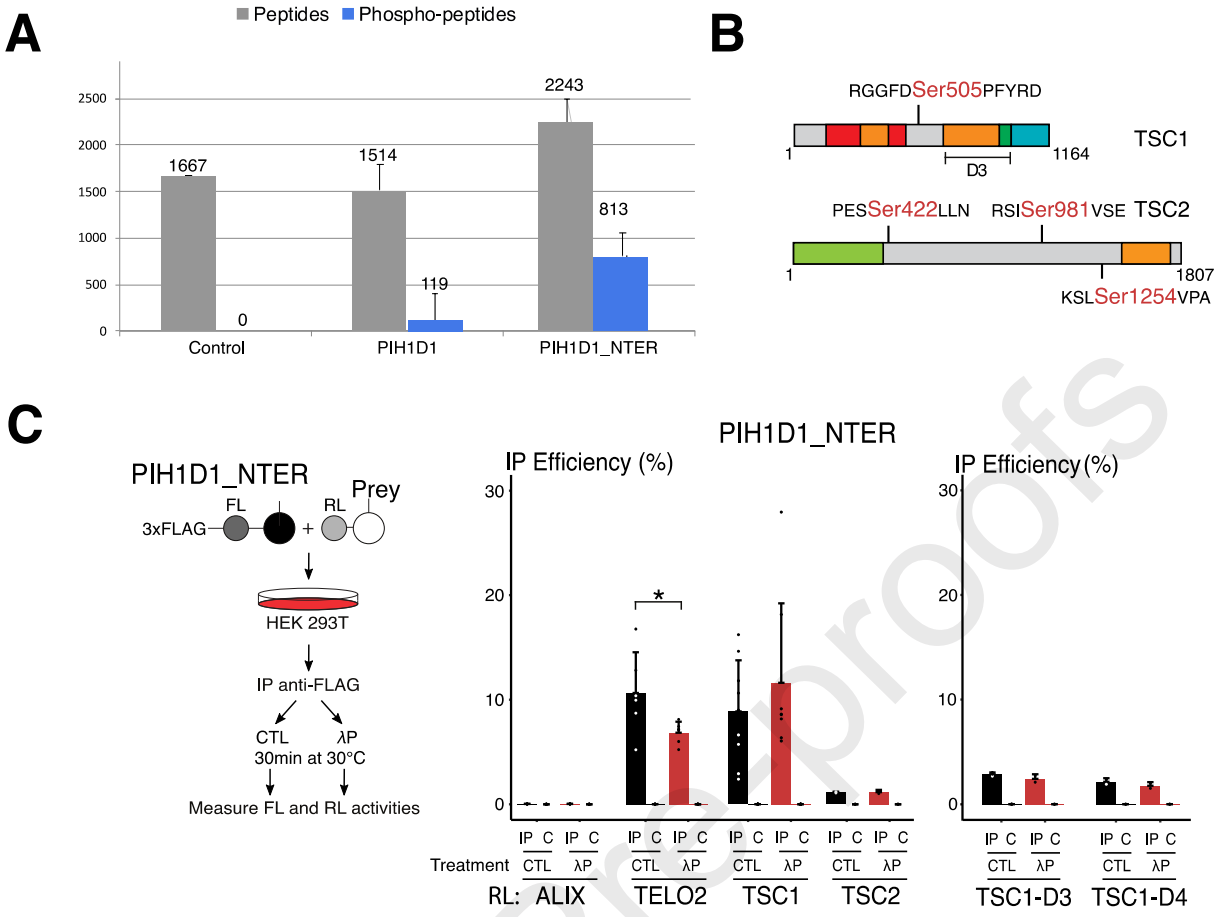

Figure 3

Figure 3. Phospho-proteomic study of PIH1D1 and PIH1D1_NTER IP and evidences that TSC1 interacts with PIH1D1_NTER

(A) Peptides and phospho-peptides detected in proteomic analysis of GFP-PIH1D1 or GFP-PIH1D1_NTER IP. CTL IP is performed with parental HeLa cells. Bars represent means of number of peptides (n=2, grey bars: total peptides, blue bars: phospho-peptides). **(B)** Schematic view of phospho-peptides detected for TSC1 and TSC2. Peptide sequences are in black and phosphorylated serines in red. **(C)** LUMIER IP showing *in vivo* interactions between PIH1D1_NTER fused to 3XFLAG-FL and TEL2, TSC1, TSC2, TSC1_D3, TSC1_D4 fused to RL in assays treated or not with lambda phosphatase after IP. ALIX fused to RL was used as a negative control of IP and TEL2 fused to RL as a positive control for lambda phosphatase effect. Left panel: schematic representation of the assay. Middle and right panels: graphs plotting the IP efficiency of the indicated proteins. Black bars are means of measures without lambda phosphatase (CTL) and red bars with lambda phosphatase (λP). Bars represent the mean. Experiments were repeated 5 or 6 times and each experiment itself contained two replicates. Error bars: standard deviation. Stars: values significantly different with * = p-value < 0.05 (Student t-test).

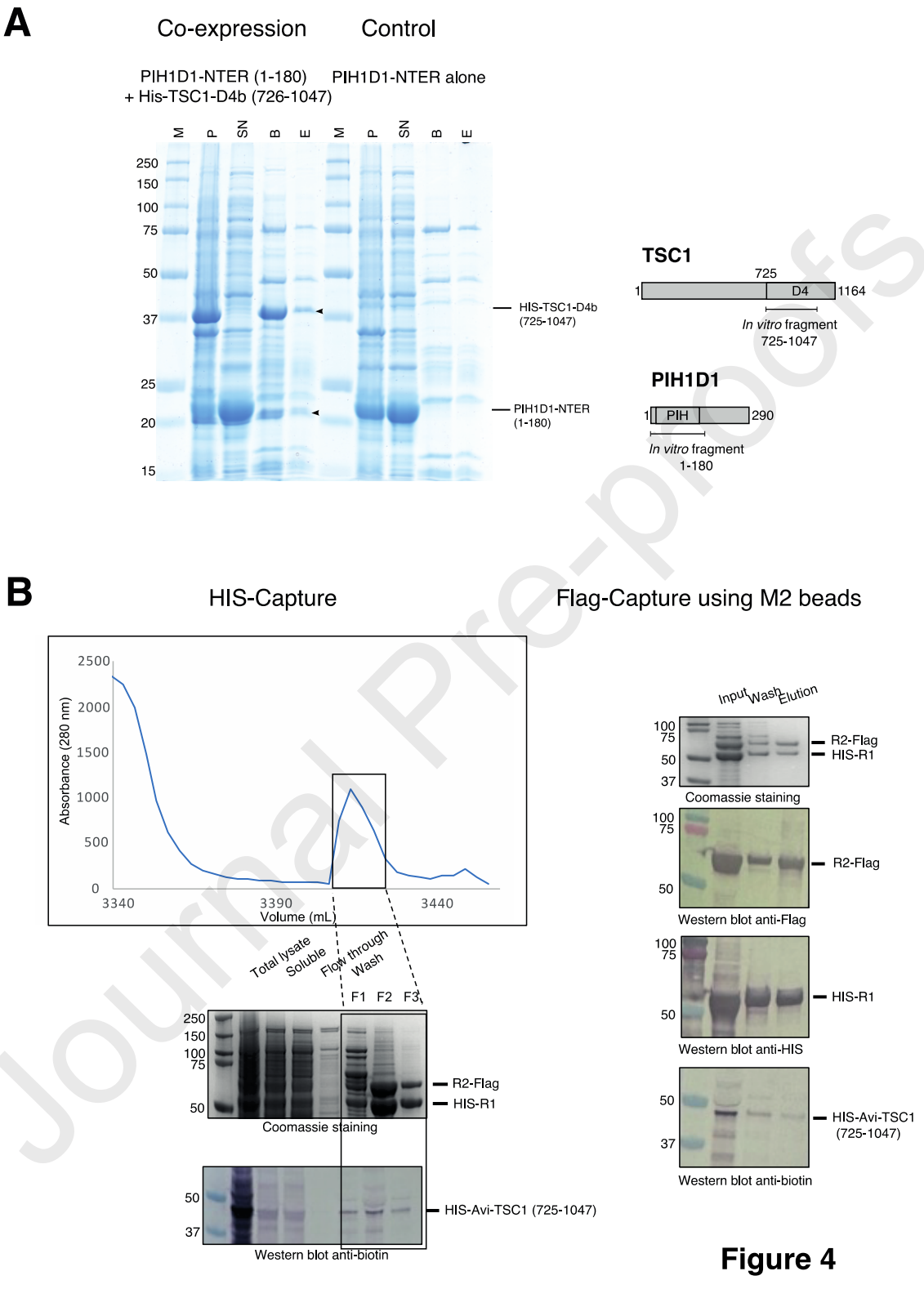

Figure 4

Figure 4. TSC1 makes direct interaction with PIH1D1_NTER and RUVBL1/2

(A) Coomassie-stained SDS-PAGE 10% of His-TSC1-D4b (725-1047) co-expressed with PIH1D1_NTER (1-180) in *E. coli* and purified on TALON resin. PIH1D1_NTER alone does not bind on resin (Control). From left to right for the two parts of the gel (Co-expression and Control): M: size of the markers in kDa; P: pellet; SN: soluble fraction; B: bound on resin; E: imidazole eluate. The position of the fragments after migration is shown on the right of the gel and a drawing of the two proteins indicates the extremities of the fragments expressed. The two arrowheads indicate the bands that were sliced from the gel to analyse their composition by proteomics (Supp Figure 3). **(B)** Co-expression of HIS-TSC1(725-1047) with HIS-RUVBL1 and RUVBL2-FLAG and successive affinity purifications targetting the tags of the different protein constructs followed by SDS-PAGE analysis. F1-3 are referring to the fractions collected for the highlighted peak and used for Flag capture. Western Blots with anti-HIS, anti-FLAG and anti-Biotin are shown. Proteins detected are indicated on the right and marker molecular weight on the left of each blot (kDa).

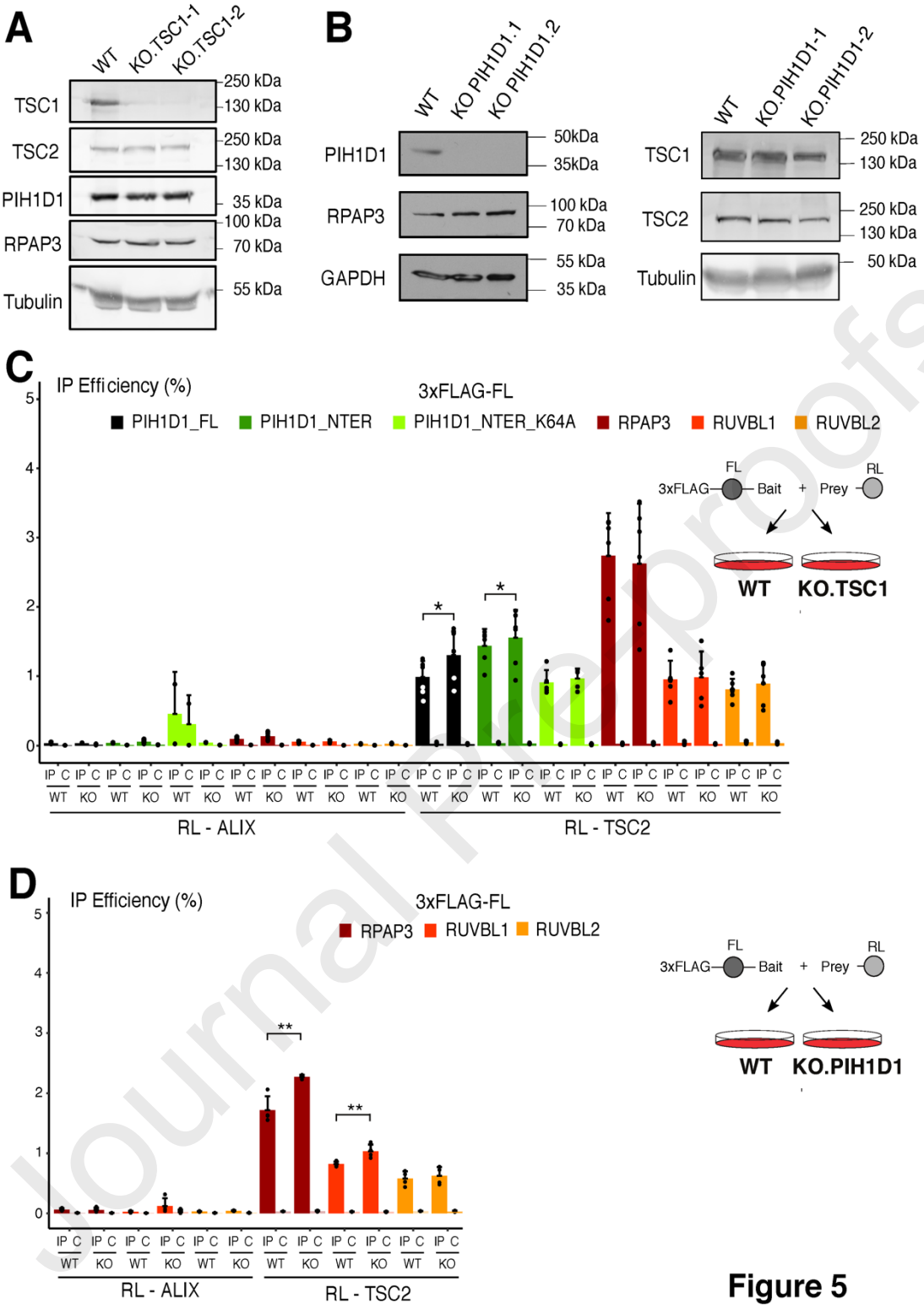

Figure 5

Figure 5. TSC2/R2TP interaction is TSC1 and PIH1D1 independent

(A) Protein level detected by Western Blot with HEK 293T parental cell extract (WT) and two TSC1.KO clone extracts (KO.TSC1-1 and KO.TSC1-2). Proteins detected are indicated on the left and marker molecular weight on the right of each blot. Tubulin is used as a loading control. **(B)** Protein level detected by Western Blots with HEK 293T parental cell extract (WT) and two PIH1D1.KO clone extracts (KO.PIH1D1-1 and KO.PIH1D1-2). Legend as in A. **(C,D)** LUMIER IP showing *in vivo* interaction between R2TP subunits fused to 3XFLAG-FL and TSC2 fused to RL in both WT or KO.TSC1 cells (C) or in both WT or KO.PIH1D1 cells (D). WT and KO cells were co-transfected with a plasmid coding for the bait (color code indicated on the top of the graph) and a plasmid coding for the prey (indicated below the graph) and anti-Flag IP is performed after 48 h. The graph plots the IP efficiency of the indicated proteins. ALIX fused to RL was used as a negative control. Experiments were repeated 5 or 6 times and each experiment itself contained two replicates. Legend as in Fig 2A.

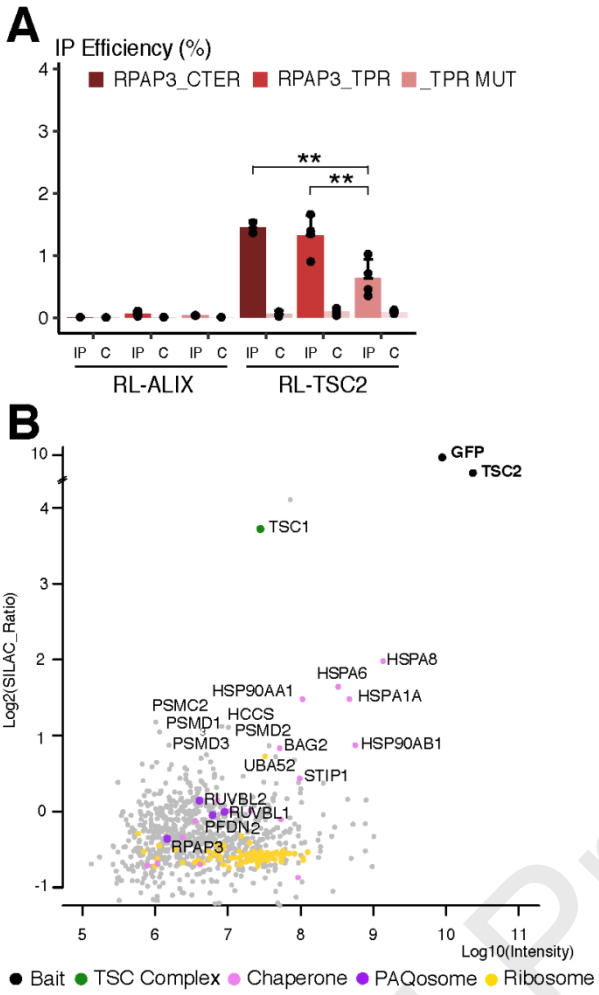

Figure 6

Figure 6. Interaction of TSC2 with RPAP3 and role of HSP90 for the stability of TSC1 and TSC2

(A) LUMIER IP showing *in vivo* interaction between RPAP3_CTER, RPAP3_TPR and RPAP3_TPR-MUT fused to 3XFLAG-FL with TSC2 fused to RL. Experiments were repeated 4 times and each experiment itself contained two replicates. Legend as in Fig 2A. **(B)** SILAC IP proteomic analysis of GFP-TSC2. The graph depicts the log2 of SILAC ratio (y axis) as a function of log10 of intensity (x axis). Stable HeLa cells expressing GFP-TSC2 were used for IP and parental cells for control IP. Each dot is a protein and the color code is indicated below the graph. **(C)** Stability of proteins upon HSP90 inhibition. Bars represent average expression level proteins indicated below the graph measured by luminescence after inhibition of HSP90 with geldanamycin (GA) compare to non-treated condition (% of expression of RL level in cells after GA treatment compared to non-treated cells, n=3). HEK 293T cells are co-transfected with plasmids coding each RL-protein and a pCMV-FL plasmid used to normalize. ALIX, CSRP2, MAP4 and RTCB were used as negative controls and NOP58 as a positive control. Error bars: standard deviation. Stars: values significantly different with *** = p-value < 0.001; ** = p-value < 0.01 (Student t-test).

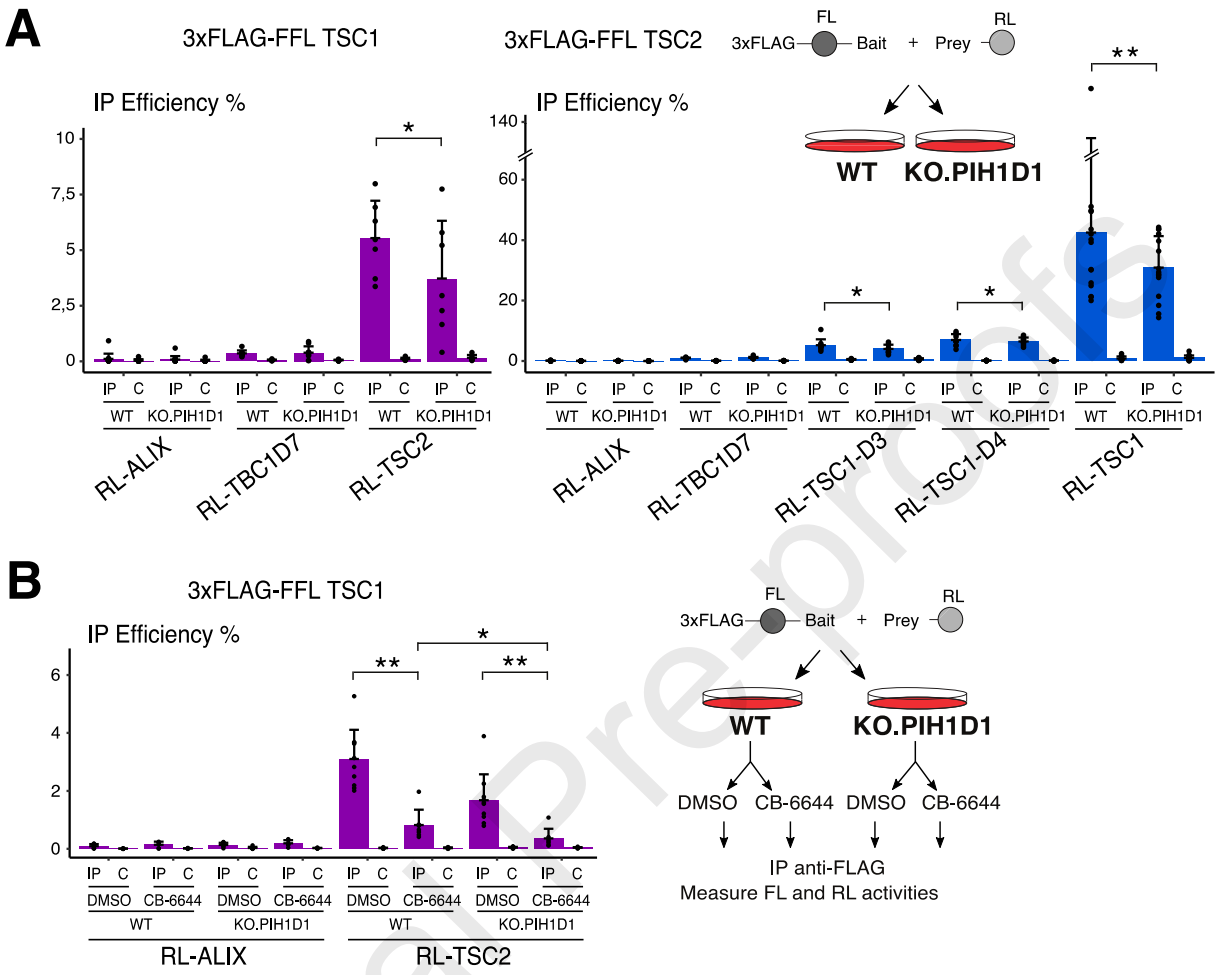

Figure 7

FIGURE 7. The absence of PIH1D1 and the inhibition of RUVBL1/2 decrease the interaction between TSC1 and TSC2.

(A) LUMIER IP showing *in vivo* interaction between TSC subunits in presence (WT) or absence of PIH1D1 (KO.PIH1D1). Left panel: graph plotting the IP efficiency of TSC1 fused to 3XFLAG-FL. Right panel: graph plotting the IP efficiency of TSC2 fused to 3XFLAG-FL. The preys fused to RL are indicated below the graphs. Experiments were repeated 6 or 7 times and each experiment itself contained two replicates. Legend as in Fig 2A. **(B)** LUMIER IP showing *in vivo* interaction between TSC subunits in the presence (WT) or absence of PIH1D1 (KO.PIH1D1) with an additional treatment by RUVBL1/2 ATPase inhibitor CB6644 or DMSO as control. Experiments were repeated 6 or 7 times and each experiment itself contained two replicates. Legend as in Fig 2A.

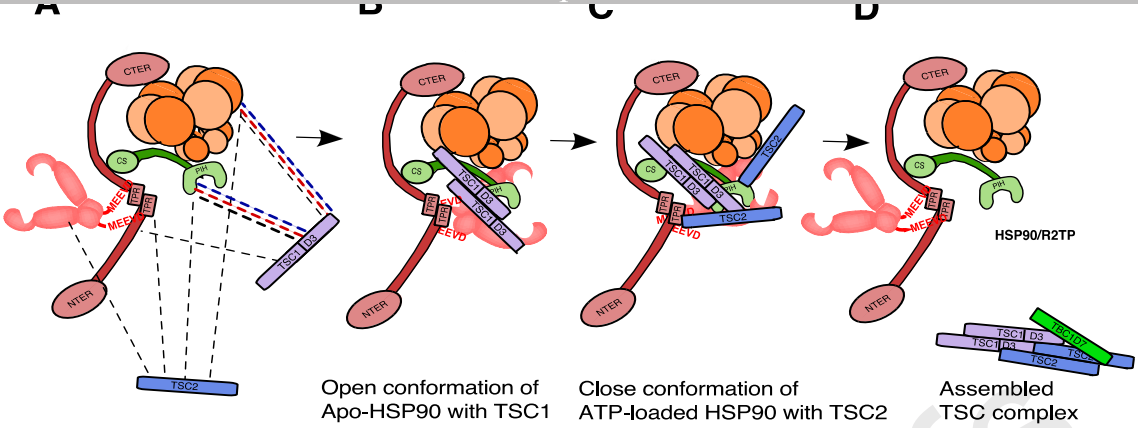

Open conformation of Apo-HSP90 with TSC1

Close conformation of ATP-loaded HSP90 with TSC2

Assembled TSC complex

Figure 8. Model showing the role of HSP90/R2TP in TSC complex assembly.

(A) Scheme showing the interaction of TSC1 and TSC2 with the R2TP subunits. Black dashed lines are interactions seen by LUMIER IP, red dashed lines seen by two-hybrid assay and blue dashed line seen in *in vitro* reconstituted assay. Thickness of the line is function of the strength of the interaction. Only one TSC1 and one TSC2 are shown to simplify. RPAP3 is represented in a non-scaled manner to give more clarity on the model **(B)** Two TSC1 bind to PIH pocket in PIH1D1 and Apo form of HSP90 **(C)** Two TSC2 bind ATP-loaded HSP90 in a close conformation and subunits of R2TP. **(D)** A rearrangement driven by ATP hydrolysis by RUVBL1/2 ATPase leads to contact between dimers of TSC1 and TS2 and release of the TSC complex that also includes TBC1D7.

Graphical Abstract

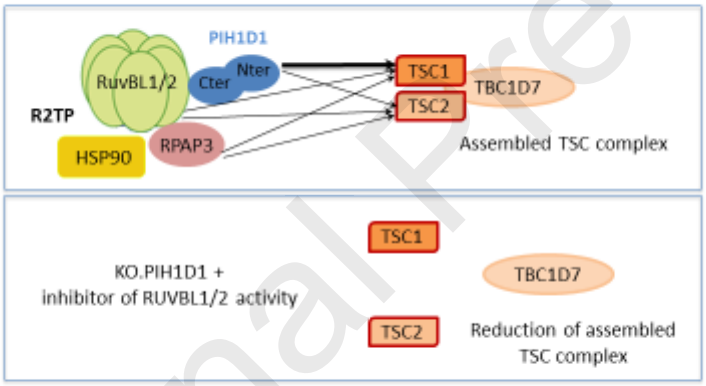

Highlights:

- TSC1 directly interacts with the N-terminal binding pocket of PIH1D1 in a phosphorylation independent manner
- Inhibition of R2TP leads to a reduction of TSC assembly
- HSP90/R2TP assemble not only mTORC1 but also its main regulator, the TSC complex

Table legends

Table S1. Label-free proteomic analyses after IP of GFP-PIH1D1, GFP-PIH1D1_NTER.

Table S2. Phospho-proteomic analysis of GFP-PIH1D1 or GFP-PIH1D1_NTER IP

Table S3. SILAC IP proteomic analysis of GFP-TSC2

Declaration of interests

☒ The authors declare that they have no known competing financial interests or personal relationships that could have appeared to influence the work reported in this paper.

☐The authors declare the following financial interests/personal relationships which may be considered as potential competing interests: